Doctoral theses at NTNU, 2013:202

Xiaoju Du

Numerical Solvers for Transient Two-Phase Flow

Doctoral Thesis

Xiaoju Du

ISBN 978-82-471-4518-0 (printed version)
ISBN 978-82-471-4519-7 (electronic version)
ISSN 1503-8181

NTNU – Trondheim
Norwegian University of Science and Technology

NTNU – Trondheim
Norwegian University of Science and Technology

NTNU
Norwegian University of Science and Technology
Thesis for the degree of Philosophiae Doctor
Faculty of Engineering Science & Technology
Department of Energy and Process Engineering

Doctoral theses at NTNU, 2013:202

NTNU

Xiaoju Du

Numerical Solvers for Transient Two-Phase Flow

Thesis for the degree of Philosophiae Doctor

Trondheim, June 2013

Norwegian University of Science and Technology
Faculty of Engineering Science & Technology
Department of Energy and Process Engineering

NTNU – Trondheim
Norwegian University of
Science and Technology

NTNU
Norwegian University of Science and Technology

Thesis for the degree of Philosophiae Doctor

Faculty of Engineering Science & Technology
Department of Energy and Process Engineering

ISBN 978-82-471-4518-0 (printed version)
ISBN 978-82-471-4519-7 (electronic version)
ISSN 1503-8181

Doctoral theses at NTNU, 2013:202

Printed by Skipnes Kommunikasjon as

Abstract

Certain numerical methods have been well developed for solving one-dimensional two-phase flow (e.g. gas and liquid) problems in the literatures during the last two decades. Based on the existing methods, the present work compares the computational efficiency, accuracy, and robustness of various numerical schemes by predicting the numerical solutions of fluid properties for a specific case to find the proper numerical method.

One of the numerical schemes introduced in this work is a practical, semi-implicit upwind method used for fluid flow simulations in different flow patterns, stratified flow and slug flow. This method implements the iterative and non-iterative schemes using a two-fluid model that consists of sets of non-hyperbolic equations. A numerical error term is applied in the pressure equation to maintain the volume balance of the two-phase flow model. If the temperature varies, the discretised energy equations use similar error terms as in the pressure equation. In some cases, the small values of the numerical errors are negligible and do not influence the numerical results. These errors are, however, important factors to consider when maintaining the stability and robustness of the above numerical schemes for strong non-linear cases. The computational efficiency of the non-iterative scheme, where the inner iterations are deactivated, is better than the iterative scheme.

Different grid arrangements are compared with respect to computational accuracy and efficiency. A staggered structured grid implements the same semi-implicit upwind method as in the non-iterative scheme; the non-staggered grid arrangement uses an existing flux-splitting scheme (Evje and Flåtten, 2003) as a reference.

All the above schemes produce numerical solutions with a single precision that normally satisfy the requirements of computational accuracy of industrial two phase pipe flows. However, if one pursues a higher-order accuracy scheme, e.g. a Roe-averaged algorithm, the governing equations should be strictly a hyperbolic system of partial differential equations, which is achieved by introducing the nonviscous force terms in the two-fluid model (LeVeque, 2002). By properly incorporating the non-conservative terms in the formulation of the

numerical fluxes, the capability of the Roe-averaged algorithm is demonstrated by capturing shock waves.

Results from the present research include the following. A one-dimensional scheme that solves a system of discretised equations with the staggered semi-implicit upwind method is presented and validated for its computational efficiency and robustness. This scheme can be widely used in the industry with sufficient accuracy. The other first-order semi-implicit numerical schemes produce stable numerical results, especially in the dynamic cases of two-phase flow, except when the gas phase nearly disappears or appears in pipes. The Roe-averaged algorithm is recommended due to the high-resolution numerical results obtained, but at the costs of computational time and effort.

Acknowledgements

I am grateful to everyone who contributed to the progress of this PhD thesis.

This project is primarily sponsored by ENI. My deepest appreciation goes to my supervisor, Professor Ole Jørgen Nydal, for offering this opportunity to me, for his sustained help and patient tuition throughout the work, and for inspiring me on a wide range of topics regarding the research direction in the field of multiphase flow.

The first person to lead me to the world of computational fluid dynamics was Professor Hemant Kamath[1], who was the supervisor of my master's study and passed away some years ago. His influence will continue to impact my whole life.

I would like to express my heart felt thanks to Mr. Keld Lund Nielsen, project manager at ENI, for encouraging and helping me when Professor Nydal was abroad during my second year. I also appreciate the warm help from Dr. Stein Tore Johansen during that period.

I would like to extend my sincere gratitude to Dr. Svend Tollak Munkejord for useful suggestions regarding the high resolution scheme; and Dr. Tore Flåtten, for generously giving advice and checking the matrices in that section.

In the Department of Energy and Process Engineering at NTNU, I experienced a friendly and fun atmosphere that made me joyful and relaxing during my stay there. Ms. Gerd Randi Fremstad, Ms. Toril Larssen, Ms. Anita Yttersian, and Ms. Gunhild Valsø Engdal were always kind, helpful, and thoughtful in giving administrative assistance; Mr. Eugen Uthaug and Mr. Ole Martin Hansen were so kind to give me a hand whenever computer or software problems were encountered. I will not forget all our kind members in Professor Nydal's group, and my special thanks to Dr. Angela De Leebeeck, who has been such a good colleague and friend.

Last but not least, the complete support from my family and friends makes me a lucky woman.

[1] 08.06.1958-30.06.2006

Contents

Nomenclature

Roman Symbols

A	First virial coefficient	$[-]$
B	Second virial coefficient	$[-]$
b	Element of known terms	
C	Third virial coefficient	$[-]$
c_g	Sound speed for gas	$[\mathrm{m/s}]$
c_l	Sound speed for liquid	$[\mathrm{m/s}]$
F	Momentum flux	$[\mathrm{kg \cdot m^2/s^2}]$
F_k^{int}	Interfacial frinction force	$[\mathrm{N}]$
f_k^{int}	Interfacial friction force divided by $(u_g - u_l)$	$[\mathrm{N \cdot s/m}]$
F_k^{nv}	Non-viscous part of interfacial friction force for phase k	$[\mathrm{N}]$
F_k^{v}	Viscous part of interfacial friction force	$[\mathrm{N}]$
f_k	Phase wall friction divided by velocity	$[\mathrm{N \cdot s/m}]$
f_w	Wall friction divided by velocity	$[\mathrm{N \cdot s/m}]$
G	Gravity force	$[\mathrm{N}]$
G_k	Phase gravity force	$[\mathrm{N}]$
I	Mass flux	$[\mathrm{kg \cdot m/s}]$
K	Bulk modulus fluid elasticity	$[\mathrm{N/m^2}]$
k	Virtual mass coefficient	$[-]$
m_k	Phase mass per unit volume	$[\mathrm{kg/m^3}]$
N	Total number cells of grid	$[-]$
P	Pressure	$[\mathrm{Pa}]$

R	Gas constant	$[\,\mathrm{J/mol/K}]$
s	Wave speed	$[\,\mathrm{m/s}]$
t	Time	$[\,\mathrm{s}]$
u	Velocity	$[\,\mathrm{m/s}]$
u_g	Gas velocity	$[\,\mathrm{m/s}]$
u_k	Phase velocity	$[\,\mathrm{m/s}]$
u_l	Liquid velocity	$[\,\mathrm{m/s}]$
x	Distance	$[\,\mathrm{m}]$
$\mathcal{C}$	Coefficients	
$\mathcal{C}_{u,g}^{u_g}$	Coefficient of gas velocity in gas momentum equation	$[\,\mathrm{kg/s}]$
$\mathcal{C}_{u,l}^{u_l}$	Coefficients of liquid velocity in liquid momentum equation	$[\,\mathrm{kg/s}]$
$\mathcal{C}_P$	Coefficient of pressure in pressure equation	$[\,-]$
$\mathcal{C}_{m,g}$	Coefficient of gas mass in gas continuity equation	$[\,\mathrm{s}^{-1}]$
$\mathcal{C}_{m,l}$	Coefficients of liquid mass in liquid continuity equation	$[\,\mathrm{s}^{-1}]$

Greek Symbols

α_g	Volume fraction for gas	$[\,-]$
α_k	Volume fraction for phase k	$[\,-]$
α_l	Volume fraction for liquid	$[\,-]$
χ_p	Compressibility factor	$[\,\mathrm{Pa}^{-1}]$
δ	Numerical error term	
ϵ	Preassigned small numbers	
ρ	Mass per unit volume	$[\,\mathrm{kg/m}^3]$
ρ_k	Density for phase k	$[\,\mathrm{m/s}]$

Vectors and Matrices

$\mathbf{\Lambda}$	Eigenvalues of matrix $\mathbf{A}$
$\mathbf{A}$	Jacobian matrix of conservative fluxes F
$\mathbf{B}$	Matrix of coefficients of non-conservative terms

$\mathbf{b}$	Known terms vector
$\mathbf{C}$	Coefficient matrix in Section 3.4.1
$\mathbf{F}$	Vector of fluxes
$\mathbf{Q}$	Vector of conservative variables
$\mathbf{R}$	Right eigenvector of matrix $\mathbf{A}$
$\mathbf{R}^{-1}$	Left eigenvector of matrix $\mathbf{A}$
$\mathbf{S}$	Vector of sources
$\mathbf{U}$	Vector of non-conservative variables
$\mathbf{V}$	Vector of primitive variables
$\mathbf{x}$	Unknown variables vector
F	Vector of non-conservative fluxes
$\mathcal{F}$	Vector of conservative fluxes

Superscripts

$'$	Correction of variables
$+$	Positive, see equation (4.46)
$-$	Minus, see equation (4.46)
$*$	Fluxes solved semi-implicitly
$\dagger$	Time step n or $n+1$
$\ddagger$	Guessed values of variables
i	Iterative step in inner loop
int	Interfacial
L	Left state
n	Time level
nv	Non-conservative terms introduce by non-viscous interfacial friction force
P	Coefficient of pressure
p	Pressure gradient term
R	Right state

u_g	Coefficient of gas velocity
u_l	Coefficient of liquid velocity
v	Viscous

Subscripts

$+$	Forward, see equation (4.43)
$-$	Backward, see equation (4.44)
0	Initial
g	Gas
I	Interface flux, see equation (4.45)
J	Spatial index at interface, same as $j - 1/2$
j	Spatial index at cell centre
k	Gas or liquid
L	Left state in sections 4.1 and 4.2
l	Liquid
P	Pressure equation
R	Right state in sections 4.1 and 4.2
t	Derivative with respect to time
u	Momentum equation
w	Wall
x	Derivative with respect to space

Mathematical Symbols

Δ	Computational interval/change in
∂	Partial derivative

Fundamental Numerical Methods for Two-Phase Flow

1. Introduction

1.1. Two-phase flow in pipes

Two-phase flow occurs frequently in many industrial applications. Separating, storing, and transporting oil and gas is of particular importance in offshore oil/gas recovery. The flow systems become complex because of the existence of various flow regimes. Large scale transient flow can be activated by a start-up or a shut-down operation. Severe riser slugging is a slow phenomenon, and pressure propagation is a rapid phenomenon. Different flow patterns depend on the combinations of the flow rates, pipe geometry, and fluid properties (Ishii and Hibiki, 2006). The general classifications include separated flows (including stratified flow), transitional or mixed flows (including slug flow), and dispersed flows (Ishii and Hibiki, 2006). In this work, stratified flow is primarily considered, for simplicity, and the transition to slug flow is explored in one instance. Slug flow forms from unstable stratified flow or in bends.

It is summarised in the thesis of Munekjord (Munekjord, 2006) how the mathematical models of two-phase flow are established by averaging the single-phase flow model. Some numerical methods have been well developed for solving two-phase flows (Prosperetti and Tryggvason, 2009). The goal is to establish a robust, efficient, and accurate numerical scheme. In this work, these three advantages cannot exist simultaneously in one numerical scheme; however, it remains an ambition for the future. A useful numerical scheme can be recommended to other researchers.

The choice of the numerical method partially depends on the flow characteristics, including compressibility of the fluids, the flow patterns, the complexity of geometries, etc. Certain methods can be applied to specific phenomena, such as different flow regimes, phase appearance and disappearance, and interface tracking in droplets and liquid films, while the numerical capabilities of other methods are impeded in those situations.

In the present work, while neglecting the difficulties introduced by different flow patterns, finite-volume methods are applied on the partial differential equations of compressible transient two-phase flows in one-dimensional domains.

During the linearisation procedure, the integrals of the partial differentiation with respect to time can be estimated implicitly or explicitly. In the explicit numerical schemes, the stability requires the time step to satisfy the Courant-Friedrichs-Lewy (CFL) condition. However, the fully implicit schemes increase computational cost due to introduced non-linear terms, but provide unconditional stability. One compromise is the utilisation of a semi-implicit scheme that is capable of violating the CFL condition, and with or without inner iterations at one time step. The semi-implicit schemes are stable and robust, even when using large time steps, which is beyond the capability of explicit schemes (Prosperetti and Tryggvason, 2009). An upwind method is widely used to solve the diffusive fluxes because of its simplicity, and a "false diffusive"(Versteeg and Malalasekera, 1995) profile can be obtained by this method when there is a contact discontinuity or shock occurring in the fluid flows. At such a point, some high-resolution schemes have been developed and validated, such as the flux limiter and Roe-averaged algorithms. Because of the strong coupling between pressure and velocity, or between mass and velocity in the numerical computation of multiphase flow, the staggered and non-staggered grid arrangements (Versteeg and Malalasekera, 1995) produce slightly different profiles of fluid properties along the pipes with inclinations.

1.2. Comparisons of numerical schemes

In the comparison of the accuracy, robustness, and computational efficiency of the existing numerical schemes for the two-fluid model, we focus primarily on three numerical issues based on the assumpation of constant temperature:

- The non-iterative versus iterative schemes using the semi-implicit upwind method. In this numerical issue, cases involved with energy equation are tested except for constant temperature cases, and a sub-issue, simultaneous versus sequential schemes, is dicussed.
- Staggered (semi-implicit upwind method) versus non-staggered (Evje and Flåtten, 2003) grid arrangements.
- The first-order explicit scheme (FORCE2 scheme with Lax-Friedrichs flux and Richtmyer flux) versus high-resolution scheme (Roe-averaged algorithm with MUSCL-Hancock procedure).

The robustness and efficiency of the non-iterative scheme is validated, and it is not as accurate as the iterative scheme. The staggered grid arrangement generates more diffusive profiles than the non-staggered grid arrangement at the discontinuities in fluid flows. The high-resolution scheme demonstrates an

accuracy improvement, compared with the first-order schemes. Additionally, numerical tests have been made on single-phase isothermal flow, single-phase thermal flow, and two-phase thermal flow in a one-dimensional domain.

1.3. Overview of thesis

This thesis is organised in the following manner. A short introduction is presented in this Chapter. The next chapter introduces the governing equations of two-phase flow models. The relevant numerical methods for solving the mathematical models are described in Chapter 3 and Chapter 4. Chapter 5 presents the results and the discussion. Chapter 6 provides the concluding remarks. Appendix A describes the expressions of the friction forces used in the two-phase flow computation. The LU-factorisation method is briefly presented in Appendix B. All three parts of the nonviscous interfacial forces that ensure the existence of real eigenvalues and eigenvectors are described in Appendix C. Appendix D presents the details of the matrices required for the Roe-averaged algorithm used in the two-phase flow model.

2. Mathematical equations for the two-phase flow model

The governing equations are generalised for two-phase flows in one-dimension as follows:

$$\frac{\partial \mathbf{Q}}{\partial t} + \frac{\partial \mathbf{F}}{\partial x} = \mathbf{S} \tag{2.1}$$

where $\mathbf{Q}$ is the vector of conservative variables, $\mathbf{F}$ is the flux vector, and $\mathbf{S}$ is the source vector containing a mass source in the mass conservation equation and forces in the momentum equation.

2.1. Single-phase flow model

The single-phase flow model uses the mass and momentum equations for one-dimensional compressible isothermal flows. The expanded form of equation (2.1) is presented as follows:

$$\mathbf{Q} = \begin{bmatrix} \rho \\ \rho u \end{bmatrix} \quad \mathbf{F} = \begin{bmatrix} \rho u \\ \rho u^2 + P \end{bmatrix} \quad \mathbf{S} = \begin{bmatrix} 0 \\ G + f_w u \end{bmatrix} \tag{2.2}$$

The two-phase flow model can be derived by averaging the single-phase flow model over the pipe cross sections.

2.2. Non-hyperbolic two-phase flow model

The two-phase flow is derived from the mass and momentum conservation equations for each phase (in the two-fluid model). This mathematical model, containing two separate sets of conservation equations for each phase, is written as:

$$\mathbf{Q} = \begin{bmatrix} m_k \\ m_k u_k \end{bmatrix} \quad \mathbf{F} = \begin{bmatrix} m_k u_k \\ m_k u_k^2 + \bar{\alpha}_k P \end{bmatrix} \mathbf{S} = \begin{bmatrix} 0 \\ G_k + f_k^{int}(u_g - u_l) + f_k u_k \end{bmatrix} \tag{2.3}$$

The mass per unit pipe volume m_k is equal to the product of the volume fraction α_k and the density ρ_k. Expressions of the friction forces f_k and f_k^{int} are presented in Appendix A.

The volume balance is required in the two-phase flows:

$$\alpha_g + \alpha_l = 1 \tag{2.4}$$

All the governing equations in (2.3) are non-hyperbolic, and cannot be solved by a high-resolution scheme, e.g. the Roe-averaged algorithm. As a consequence, the hyperbolic equations are strictly required to solve two-phase flow problems if Roe averages are used.

2.3. Hyperbolic two-phase flow model

In a hyperbolic two-phase flow model, the complex form of the interfacial friction F_k^{int} is used, and the mathematical model is written as follows:

$$\mathbf{Q} = \begin{bmatrix} m_k \\ m_k u_k \end{bmatrix} \quad \mathbf{F} = \begin{bmatrix} m_k u_k \\ m_k u_k^2 + \bar{\alpha}_k P - F_k^{int} \end{bmatrix} \quad \mathbf{S} = \begin{bmatrix} 0 \\ G_k \end{bmatrix} \tag{2.5}$$

The interfacial friction term contains two parts, a viscous force F_k^v neglected in certain cases, and a nonviscous force. The nonviscous interfacial force is represented (Städtke, 2006) as follows:

$$\begin{aligned} F_g^{nv} \;=\; & -\alpha_g\alpha_l(\alpha_g\rho_g + \alpha_l\rho_l)k\left(\frac{\partial u_g}{\partial t} - \frac{\partial u_l}{\partial t} + u_l\frac{\partial u_g}{\partial x} - u_g\frac{\partial u_l}{\partial x}\right) \\ & +\alpha_g\alpha_l(\alpha_l\rho_g - \alpha_g\rho_l)(u_g - u_l)\left(\frac{\partial u_g}{\partial x} - \frac{\partial u_l}{\partial x}\right) \\ & -\alpha_g\alpha_l(\rho_g + \rho_l)(u_g - u_l)\left(\frac{\alpha_g}{\rho_g}\frac{\partial \rho_g}{\partial t} + \frac{\alpha_l}{\rho_l}\frac{\partial \rho_l}{\partial t}\right. \\ & \qquad \left. +u_g\frac{\alpha_g}{\rho_g}\frac{\partial \rho_g}{\partial x} + u_l\frac{\alpha_l}{\rho_l}\frac{\partial \rho_l}{\partial x}\right) \\ & -\alpha_g\alpha_l(\rho_g + \rho_l)(u_g - u_l)^2\frac{\partial \alpha_g}{\partial x} \end{aligned} \tag{2.6}$$

and $F_l^{nv} = -F_g^{nv}$. The value of the virtual mass coefficient k varies with the flow type (Städtke, 2006), i.e. k is zero for stratified flow, k is approximately equal to $1/2$ for dispersed droplet or bubbly flow, $k > 0.5$ will indicate churn-turbulent flow, and if one phase disappears, the value of k approaches infinite,

and $(u_g - u_l) \to 0$. (For a detailed description of the nonviscous interfacial forces, refer to Appendix C.)

In the stratified flow regime, the nonviscous interfacial friction force in the mathematical model described by equation (2.5) can be simplified as follows:

$$F_g^{nv} = -\alpha_g \alpha_l (u_g - u_l)(\rho_g \frac{\partial u_g}{\partial x} + \rho_l \frac{\partial u_l}{\partial x}) \tag{2.7}$$

2.4. Equations of state

The non-linear state equations can induce large numerical errors because of the incorrect compressibility factor introduced in the pressure equation. Methane (gas) and water (liquid) are considered as testing fluids for some numerical tests and are assumed to be immiscible in this work.

The state equation for water with varying pressures is defined by the website The Engineering ToolBox as follows:

$$\rho_l = \frac{\rho_{l,0}}{1 - (P - P_0)/K} \tag{2.8}$$

where the initial density of water $\rho_{l,0} = 1000\,\mathrm{kg/m^3}$, the pressure $P_0 = 101325\,\mathrm{Pa}$, and the bulk modulus fluid elasticity $K = 2.15 \times 10^{-9}\,\mathrm{N \cdot m^{-2}}$.

For the gas-phase methane, the virial state equation (Prausnitz et al., 1999) is applied under a constant temperature (273.15 K):

$$P = RT_0 \left(A\rho_g^3 + B\rho_g^2 + C\rho_g\right) \tag{2.9}$$

where the gas constant $R = 8.31451\,\mathrm{J \cdot mol^{-1} \cdot K^{-1}}$ and the coefficients are $A = 53/18/16^3$, $B = -53/16^2$, and $C = 1000/16$, which are taken from the work of Douslin (1962) on methane (Prausnitz et al., 1999).

State equations (2.8) and (2.9) are used for the first two numerical issues mentioned in the introductory Chapter 1.

For the last numerical issue, the linear equations of state for each phase are implemented as follows:

$$\rho_g = \frac{P}{c_g^2} \tag{2.10}$$

where the speed of sound $c_g^2 = 10^5\,\mathrm{m/s}$. And

$$\rho_l = \rho_{l,0} \frac{P - P_0}{c_l^2} \tag{2.11}$$

where the speed of sound $c_l = 10^3\,\mathrm{m/s}$. The parameters $\rho_{l,0}$ and P_0 are the same as in equation (2.8).

3. First-order numerical methods: semi-implicit fluxes

In the numerical computations of two-phase flows, a one-dimensional domain is normally subdivided into a finite number N cells of grid sizes $\Delta x_1, ..., \Delta x_N$. A uniform grid is adopted for simplicity, resulting in $\Delta x_1 = ... = \Delta x_N = \Delta x$. Alternatively, an irregular grid is used for computational convenience in certain cases to implement finite volume methods. Based on the uniform grid, using equation (2.1) and neglecting the source terms, a regular form of discretisation equations can be written as follows:

$$\frac{\mathbf{Q}_j^{n+1} - \mathbf{Q}_j^n}{\Delta t} + \frac{\mathbf{F}^*_{j+1/2} - \mathbf{F}^*_{j-1/2}}{\Delta x} = 0 \tag{3.1}$$

This equation is shown to be conserved by LeVeque, where the discretised equations were derived from the integral forms of the conservation equations.

If the flux term, $\mathbf{F}^*_{j+1/2}$, is evaluated explicitly, the computational capability will be limited because the scale of the direct moving distance of substances, $\Delta t|u|$, must be less than Δx, the size of each cell. Hence, the CFL condition is prescribed as follows:

$$\frac{\Delta t}{\Delta x} max_j|u| \leq 1 \tag{3.2}$$

Although the CFL condition can be violated when the fluxes are specified fully implicitly, it will cost a large amount of computational effort to calculate the resulting non-linear terms. A different way to compromise is to discretise the fluxes semi-implicitly using simple numerical methods, where large time steps can be imposed in contrast to the explicit schemes.

The upwind and other first-order precision methods are easy to implement and are capable of producing stable results. A system of linearised algebraic equations can be obtained by applying the finite volume methods to discretise the conservation equations. A general survey of two important numerical issues will be presented before applying the specific numerical methods.

3.1. Iterative versus non-iterative numerical schemes

When the word "iterative" is mentioned in the field of the computational fluid dynamics (CFD), we normally think of the numerical schemes marching in time or direct solvers converging to a solution. An additional understanding of "iterative" can be that iterations, typically called inner loop, repeat an algorithm in one time step to achieve a converged solution.

In this work, the iterative numerical scheme utilises the inner loop, but the other schemes do not. In the iterative scheme, the calculation repeats until the numerical errors are negligibly small or the converged numerical solutions are obtained at one time level. Alternatively, the numerical errors can be treated as source terms in the linearised pressure equations in the non-iterative scheme. The algorithms in this numerical issue are illustrated conceptually in Figure 3.1, and the inner loop is marked at the iterative step i by using the primitive variable u as an example.

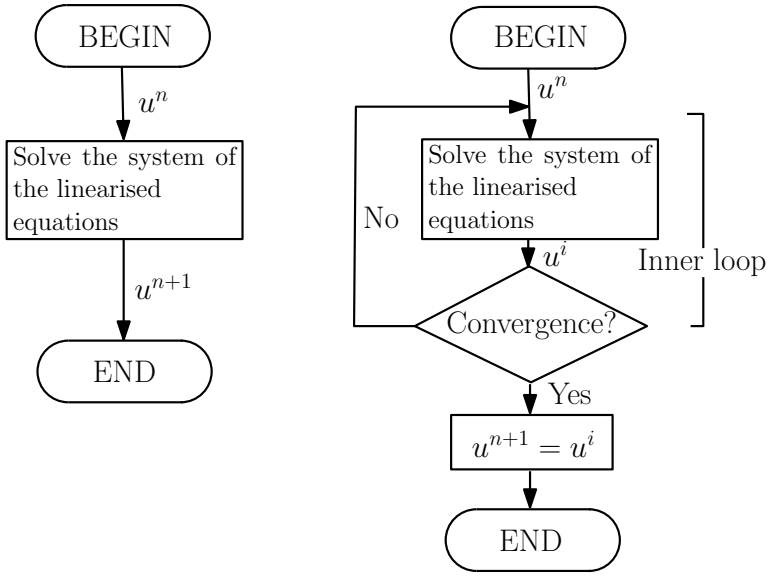

Figure 3.1.: *Non-iterative (left) versus iterative (right) schemes*

3.1.1. Convergence criterion for the iterative scheme

The convergence criterion for the iterative scheme is established on the basis of two steps. The first step is specified as follows. The maximum volume error is

limited by a pre-assigned small number ϵ_v (e.g. 10^{-6}):

$$\left|\delta v_j^i\right|_{max} \leq \epsilon_v \tag{3.3}$$

There are times when the above condition cannot be satisfied, i.e. when the solutions of the linear equations have already converged. In those instances, the additional convergence criterion is imposed (using gas velocity u_g as an example):

$$\left|u_{g,j+1/2}^{i+1} - u_{g,j+1/2}^{i}\right|_{max} \leq \epsilon_u \tag{3.4}$$

This avoids additional iterations.

The computation is carried out with single precision and is stopped if one of the criteria is satisfied in this work. To ensure the accuracy of predicted results, the first criterion has a higher priority.

3.2. Staggered versus non-staggered grid arrangements

The governing equations are discretised on the basis of simplified uniform grid cells in one-dimension, as shown in Figure 3.2. The index j, located at the cell centre, is marked by a cross. The index $j \pm 1/2$ is located at the cell interface (staggered grid is marked by a dashed line).

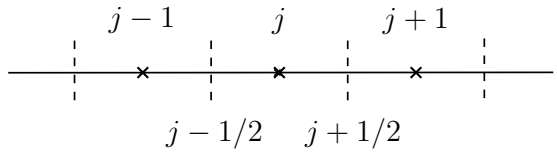

Figure 3.2.: *Grid structure.*

Dependent variables, including velocities, masses, and pressure, can be stored at the cell centre, or alternatively, at the interface. For instance, if all the variables of a mathematical model are defined at the cell centre, an inappropriate pressure gradient value participating in the numerical computation of momentum equations may lead to an irregular 'checker-board' pressure field but a uniform velocity field (Versteeg and Malalasekera, 1995). Similarly, the

same values of pressure at the cell centres contribute zero momentum sources in the discretised equations as a uniform pressure field, whereas the real pressure field can have spatial oscillations. These false behaviours can be remedied by applying a staggered grid to the velocities and pressure components, i.e. the scalar variable of velocity is stored at the cell centre, and the pressure is prescribed at the cell interface. A similar situation occurs when the grid structures of velocity and mass are non-staggered. Hence, the grid arrangement plays an important role for simulating the fluid flows in the inclined pipelines governed by the two-fluid model.

Initially, simulation tests on the staggered arrangement, called staggered gas and liquid velocities (SGL), are run with a semi-implicit upwind method. Then, as a comparison, the liquid velocity is prescribed on the non-staggered grid (staggered gas velocity and non-staggered liquid velocity (SGNSL)), based on the SGL numerical scheme. A sub-model, called steady gas equation, is used to calculate the numerical values of the pressure gradient term in the liquid momentum equation. Finally, the non-staggered grid (non-staggered gas and liquid velocities (NSGL)) for the velocity and mass components is implemented . The strongly implicit mixture flux method combined with an advection upstream splitting method (SIMF-AUSMD) developed by Evje and Flåtten, is applied in the NSGL grid arrangement.

3.3. Discretisation equations

Equation (2.3), describing the mathematical model, consists of two sets of partial differential equations for the two-phase compressible flow; each phase includes two conservation equations, the mass and momentum balance equations. In some numerical methods, the governing equations alone cannot predict the pressure implicitly through the momentum equations: for those cases, a derived pressure equation is introduced in the following section.

3.3.1. Pressure equation

The pressure equation, derived from the volume balance and mass balance equations, can be used in the numerical computation of the two-phase flow. The pressure equation for the two-fluid model (2.3) is derived in the following manner.

The phasic mass per unit volume at the time level $n+1$ is expressed as the following product:

$$m_k^{n+1} = \alpha_k^{n+1} \rho_k^{n+1} \tag{3.5}$$

Discretising the volume fraction $\alpha_k^{n+1} = \alpha_k^n + d\alpha_k$ and the density $\rho_k^{n+1} = \rho_k^n + d\rho_k$ of the product of mass in equation (3.5) is expressed as follows:

$$m_k^{n+1} = \alpha_k^n \rho_k^n + \alpha_k^n d\rho_k + \rho_k^n d\alpha_k + d\rho_k d\alpha_k \tag{3.6}$$

where $d\alpha_g = -d\alpha_l$.

In the non-iterative scheme, the second order term, $d\rho_k d\alpha_k$, is neglected, but it can be included in the iterative scheme by updating the volume fraction in the inner loop. By dividing equation (3.6) by ρ_k^n and reorganising the resulting equation, the following equation is obtained:

$$\alpha_k^n = \frac{m_g^{n+1}}{\rho_g^n} - \frac{\alpha_k^n d\rho_k}{\rho_k^n} - d\alpha_k - \frac{d\rho_k d\alpha_k}{\rho_k^n} \tag{3.7}$$

Recalling the volume balance equation (2.4) and substituting equation (3.7) into it, we obtain a balance equation for the iterative scheme:

$$\frac{m_g^{n+1}}{\rho_g^n} - \left(\alpha_g^n + d\alpha_g\right)\frac{d\rho_g}{\rho_g^n} - d\alpha_g + \frac{m_l^{n+1}}{\rho_l^n} - \left(\alpha_l^n + d\alpha_l\right)\frac{d\rho_l}{\rho_l^n} - d\alpha_l = 1 \tag{3.8}$$

Because $d\alpha_g = -d\alpha_l$, equation (3.8) becomes the following:

$$\frac{m_g^{n+1}}{\rho_g^n} - \left(\alpha_g^n + d\alpha_g\right)\frac{d\rho_g}{\rho_g^n} + \frac{m_l^{n+1}}{\rho_l^n} - \left(\alpha_l^n + d\alpha_l\right)\frac{d\rho_l}{\rho_l^n} = 1 \tag{3.9}$$

For the non-iterative scheme, the terms including $d\alpha_k$ are neglected in the above equation (3.9), resulting in the following:

$$\frac{m_g^{n+1}}{\rho_g^n} - \alpha_g^n\frac{d\rho_g}{\rho_g^n} + \frac{m_l^{n+1}}{\rho_l^n} - \alpha_l^n\frac{d\rho_l}{\rho_l^n} = 1 \tag{3.10}$$

In equations (3.9) and (3.10), the mass m_k^{n+1} is obtained from the discretised continuity equation for each phase.

In the equations of state, the density ρ_k is a function of the pressure P:

$$d\rho_k = \left(\frac{\partial \rho_k}{\partial P}\right)_{T_k} dP \tag{3.11}$$

Substituting m_k^{n+1} and $d\rho_k$ into equation (3.9) and (3.10), the pressure equation becomes as follows:

$$\chi_p dp + \Delta t\frac{1}{\rho_g}\frac{d(m_g u_g)}{dx} + \Delta t\frac{1}{\rho_l}\frac{d(m_l u_l)}{dx} = \delta v \tag{3.12}$$

The compressibility factor χ_p is defined as follows:

$$\chi_p = \frac{\alpha_g}{\rho_g}\frac{d\rho_g}{dp} + \frac{\alpha_l}{\rho_l}\frac{d\rho_l}{dp}. \tag{3.13}$$

and the volume error δv is prescribed as follows:

$$\delta v = \frac{m_g}{\rho_g} + \frac{m_l}{\rho_l} - 1. \tag{3.14}$$

Neglecting the volume error term, we obtain exactly the same pressure equation as the one used by Flåtten (2003).

If the non-linear state equations are employed, the incorrect compressibility factor, $\partial\rho_k/\partial P$, is introduced because this factor is inconsistent with the accurate gradient $d\rho_k/dP$ (if $dP \neq 0$). In figure 3.3, it is shown that an inaccurate pressure (marked by the dashed line) can be obtained with the analytical expression $\partial\rho_k/\partial P$, while the real value should be P^{n+1}. In the

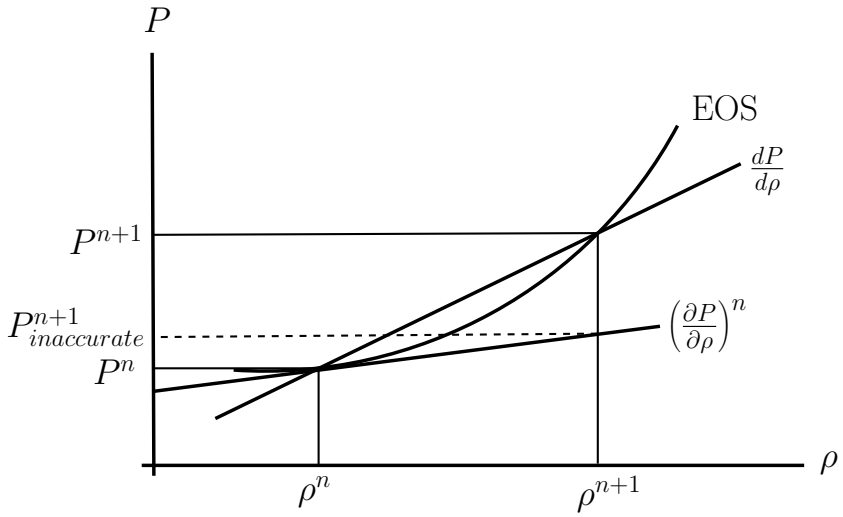

Figure 3.3.: *Pressure deviation for non-linear equation of state (EOS).*

non-iterative scheme, the gradient $\partial\rho_k/\partial P$ is applied in the pressure equation, and this inconsistency is overcome by treating the volume error as a source term. For the iterative scheme, the compressibility factor is calculated correctly by using the following expression for each phase at the iterative step i in the

inner loop:

$$\frac{d\rho}{dP} = \begin{cases} \dfrac{\rho^i - \rho^n}{P^i - P^n} & \text{if } P^i \neq P^n \\ \dfrac{\partial \rho}{\partial P} & \text{otherwise} \end{cases} \tag{3.15}$$

Simultaneously, the volume fraction α_k can also be updated in equation (3.13) in the inner loop.

3.3.2. Non-uniform structure of grid

A uniform grid Δx is popularly used in many numerical studies. However, a flexible non-uniform grid is constructed in one of the present test cases, namely, slug flow in S-shaped pipelines, and it will not change the discretisation equations. The non-uniform grid specifies the average values of mass at the cell interface by the weighted average operator:

$$m_{j+1/2} = \frac{m_j \Delta x_j + m_{j+1} \Delta x_{j+1}}{\Delta x_j + \Delta x_{j+1}} \tag{3.16}$$

x_j is equal to x_{j+1} in the uniform cells. In this work, the uniform grid arrangement is used to discretise the governing equations in the following sections for simplicity.

3.3.3. Linearised equations for the staggered grid arrangement

The variables of velocities u_g and u_l are prescribed at the cell interface, $j + 1/2$; the pressure P and masses m_g and m_l are stored at cell centre, j (refer to Figure 3.2). Therefore, the staggered grid structure exists in the coupling of pressure and velocity and in mass and velocity. The discretised equations are the following:

Gas momentum equation

$$\begin{aligned} &\frac{m^{\dagger}_{g,j-1/2} u^{n+1}_{g,j-1/2} - m^{n}_{g,j-1/2} u^{n}_{g,j-1/2}}{\Delta t} + \\ &\quad + \frac{(mu^2)^*_{g,j} - (mu^2)^*_{g,j-1}}{\Delta x} + \alpha^n_g \frac{P^{n+1}_j - P^{n+1}_{j-1}}{\Delta x} \\ &\quad = f^n_{g,j-1/2} u^{n+1}_{g,j-1/2} + f^{int,n}_{g,j-1/2} (u^{n+1}_{g,j-1/2} - u^{n+1}_{l,j-1/2}) + G^n_{g,j-1/2} \end{aligned} \tag{3.17}$$

Liquid momentum equation

$$\frac{m^{\dagger}_{l,j-1/2}u^{n+1}_{l,j-1/2} - m^{n}_{l,j-1/2}u^{n}_{l,j-1/2}}{\Delta t} + \\ + \frac{(mu^2)^{*}_{l,j} - (mu^2)^{*}_{l,j-1}}{\Delta x} + \alpha^{n}_{l}\frac{P^{n+1}_{j} - P^{n+1}_{j-1}}{\Delta x} \\ = f^{n}_{l,j-1/2}u^{n+1}_{l,j-1/2} + f^{int,n}_{l,j-1/2}(u^{n+1}_{g,j-1/2} - u^{n+1}_{l,j-1/2}) + G^{n}_{l,j-1/2} \quad (3.18)$$

Pressure equation

$$\chi^{\dagger}_{p,j}(P^{n+1}_{j} - P^{n}_{j}) + \frac{\Delta t}{\rho^{n}_{g,j}}\frac{m^{\dagger}_{g,j+1/2}u^{n+1}_{g,j+1/2} - m^{\dagger}_{g,j-1/2}u^{n+1}_{g,j-1/2}}{\Delta x} + \\ + \frac{\Delta t}{\rho^{n}_{l,j}}\frac{m^{\dagger}_{l,j+1/2}u^{n+1}_{l,j+1/2} - m^{\dagger}_{l,j-1/2}u^{n+1}_{l,j-1/2}}{\Delta x} = \delta v^{n}_{j} \quad (3.19)$$

Gas continuity equation

$$\frac{m^{n+1}_{g,j} - m^{n}_{g,j}}{\Delta t} + \frac{(m^{n+1}u^{\dagger})_{g,j+1/2} - (m^{n+1}u^{\dagger})_{g,j-1/2}}{\Delta x} = S^{n}_{g,j} \quad (3.20)$$

Liquid continuity equation

$$\frac{m^{n+1}_{l,j} - m^{n}_{l,j}}{\Delta t} + \frac{(m^{n+1}u^{\dagger})_{l,j+1/2} - (m^{n+1}u^{\dagger})_{l,j-1/2}}{\Delta x} = S^{n}_{l,j} \quad (3.21)$$

The volume fraction at the cell interface can be defined as the arithmetic average, $\alpha_{k,j-1/2} = (\alpha_{k,j-1} + \alpha_{k,j})/2$.

3.3.4. Linearised equations for the non-staggered liquid velocity

The liquid velocity is redefined at the cell centre based on the staggered grid arrangement and the coupling of liquid velocity corresponding to the masses and pressure changes in the non-staggered structure.

The liquid momentum equation is discretised at the cell centre as follows:

$$\frac{m^{\dagger}_{l,j}u^{n+1}_{l,j} - m^{n}_{l,j}u^{n}_{l,j}}{\Delta t} + \\ + \frac{(mu^2)^{*}_{l,j+1/2} - (mu^2)^{*}_{l,j-1/2}}{\Delta t} + \alpha^{n}_{l}\frac{P^{n+1}_{j+1/2} - P^{n+1}_{j-1/2}}{\Delta x} \\ = f^{n}_{l,j}u^{n+1}_{l,j} + f^{int,n}_{l,j}(u^{n+1}_{g,j} - u^{n+1}_{l,j}) + G^{n}_{l,j} \quad (3.22)$$

Equation (3.22) is sensitive to the pressure gradient term because of the non-staggered grid arrangement used for the liquid velocity. If the pressure at the cell interface is solved using the arithmetic average of the values at the centres of the neighbouring cells, the strong coupling between pressure and liquid velocity induces an instability because both variables are stored at the cell centre. A sub-model is introduced in the liquid momentum equation to rectify this issue.

First, the summation of the two-phase momentum equations provides a mixture momentum equation by cancelling the interfacial friction terms. Then, a steady gas equation is obtained from the mixture momentum equation by assuming a gas velocity constant with time (steady gas flow):

$$\frac{\partial m_l u_l}{\partial t} + \frac{\partial \left(m_g u_g^2 + m_l u_l^2\right)}{\partial x} + \frac{\partial P}{\partial x} = G_g + f_g u_g + G_l + f_l u_l \tag{3.23}$$

Disctretising the above equation obtains the following equation:

$$\begin{aligned} \frac{(m^\dagger u^{n+1})_{l,j} - (mu)^n_{l,j}}{\Delta t} &+ \frac{(mu^2)^*_{l,j+1/2} - (mu^2)^*_{l,j-1/2}}{\Delta x} + \\ &+ \frac{(mu^2)^*_{g,j+1/2} - (mu^2)^*_{g,j-1/2}}{\Delta x} + \frac{P^{n+1}_{j+1/2} - P^{n+1}_{j-1/2}}{\Delta x} \\ &= f^n_{l,j} u^{n+1}_{l,j} + f^n_{g,j} u^{n+1}_{g,j} + G^n_{l,j} + G^n_{g,j} \end{aligned} \tag{3.24}$$

Through reorganisation of equation (3.24), the pressure drop in the liquid momentum equation (3.23) results in the following:

$$\begin{aligned} \alpha^n_{l,j} \frac{P^{n+1}_{j+1} - P^{n+1}_{j-1/2}}{\Delta x} = &-\alpha^n_{l,j} \frac{(m^\dagger u^{n+1})_{l,j} - (mu)^n_{l,j}}{\Delta t} - \\ &- \alpha^n_{l,j} \frac{(mu^2)^*_{l,j+1/2} - (mu^2)^*_{l,j-1/2}}{\Delta x} - \\ &- \alpha^n_{l,j} \frac{(mu^2)^*_{g,j+1/2} - (mu^2)^*_{g,j-1/2}}{\Delta x} + \\ &+ \alpha^n_{l,j} f^n_{l,j} u^{n+1}_{l,j} + \alpha^n_{l,j} f^n_{g,j} u^{n+1}_{g,j} + \alpha^n_{l,j} G^n_{l,j} + \alpha^n_{l,j} G^n_{g,j} \end{aligned} \tag{3.25}$$

The pressure drop equation (3.25) is substituted into the liquid momentum equation (3.22) to avoid the strong pressure-velocity (liquid) coupling:

Liquid momentum equation

$$\alpha_{g,j}^n \frac{m_{l,j}^\dagger u_{l,j}^{n+1} - m_{l,j}^n u_{l,j}^n}{\Delta t} + \alpha_{g,j}^n \frac{(mu^2)_{l,j+1/2}^* - (mu^2)_{l,j-1/2}^*}{\Delta t} - \\ - \alpha_{l,j}^n \frac{(mu^2)_{g,j+1/2}^* - (mu^2)_{g,j-1/2}^*}{\Delta x} = \alpha_{g,j}^n f_{l,j}^n u_{l,j}^{n+1} - \alpha_{l,j}^n f_{g,j}^n u_{g,j}^{n+1} + \\ + f_{l,j}^{int,n}(u_{g,j}^{n+1} - u_{l,j}^{n+1}) + \alpha_{g,j}^n G_{l,j}^n - \alpha_{l,j}^n G_{g,j}^n \quad (3.26)$$

Another method found in the literature (H. Paillère and Cascales; Liou) to eliminate this instability is to use an ASUM+ scheme for the pressure gradient term in the non-staggered liquid momentum equation. This ASUM+ scheme requires fine meshes, which are not available for our cases at this time. Large grid sizes are tested in the existing numerical schemes, which are more efficient and preferable for practical and real applications.

3.3.5. Linearised equations of the non-staggered structure for mass and velocity (SIMF-AUSMD)

The variables of the masses and velocities, prescribed on the cell centre, indicate the non-staggered grid arrangement between them. By combining with the Lax-Friedrichs method in the pressure equation, a staggered pressure is taken into account by Flåtten:

Pressure equation

$$\chi_{j+1/2}^n \frac{P_{j+1/2}^{n+1} - \frac{1}{2}(P_j^n + P_{j+1}^n)}{\Delta t} + \\ \frac{1}{\rho_{g,j+1/2}^n} \frac{I_{g,j+1}^{n+1} - I_{g,j}^{n+1}}{\Delta x} + \frac{1}{\rho_{l,j+1/2}^n} \frac{I_{l,j+1}^{n+1} - I_{l,j}^{n+1}}{\Delta x} = 0 \quad (3.27)$$

Gas momentum equation

$$\frac{I_{g,j}^{n+1} - I_{g,j}^n}{\Delta t} + \frac{(Iu)_{g,j+1/2}^* - (Iu)_{g,j-1/2}^*}{\Delta x} + \alpha_g^n \frac{P_{j+1/2}^{n+1} - P_{j-1/2}^{n+1}}{\Delta x} \\ = f_{g,j}^n u_{g,j}^{n+1} - f_{i,j}^n (u_{g,j}^{n+1} - u_{l,j}^{n+1}) + G_{g,j}^n \quad (3.28)$$

Liquid momentum equation

$$\frac{I_{l,j}^{n+1}-I_{l,j}^{n}}{\Delta t}+\frac{(Iu)_{l,j+1/2}^{*}-(Iu)_{l,j-1/2}^{*}}{\Delta x}+\alpha_l^n\frac{P_{j+1/2}^{n+1}-P_{j-1/2}^{n+1}}{\Delta x} = f_{l,j}^{n}u_{l,j}^{n+1}+f_{i,j}^{n}(u_{g,j}^{n+1}-u_{l,j}^{n+1})+G_{l,j}^{n} \tag{3.29}$$

Gas Continuity equation

$$\frac{m_{g,j}^{n+1}-m_{g,j}^{n}}{\Delta t}+\frac{I_{g,j+1/2}^{*}-I_{g,j-1/2}^{*}}{\Delta x}=S_{g,j}^{n} \tag{3.30}$$

Liquid Continuity equation

$$\frac{m_{l,j}^{n+1}-m_{l,j}^{n}}{\Delta t}+\frac{I_{l,j+1/2}^{*}-I_{l,j-1/2}^{*}}{\Delta x}=S_{l,j}^{n} \tag{3.31}$$

The mass fluxes are expanded as $I_k = m_k u_k$. In addition, the velocity components in the friction terms are treated as $u_k^{n+1} = I_k^{n+1}/m_k^n$. The reason for keeping the integrated form of mass fluxes is for computational convenience when utilising the flux-splitting method.

3.4. Algorithm of the semi-implicit upwind scheme

A drawback of the upwind numerical method is the "diffusive-like" (mentioned by Versteeg and Malalasekera) profiles, especially for a shock tube, but this effect can be improved by grid refinement.

By recalling equations (3.17), (3.18), and (3.19) with a staggered grid arrangement, the fluxes are solved as follows:

$$(mu^2)_{k,j}^{*}=\begin{cases}(m^{\dagger}u^{n})_{k,j-1/2}u_{k,j-1/2}^{n+1} & \text{if } u_{k,j+1/2}^{n}+u_{k,j-1/2}^{n}>0\\ (m^{\dagger}u^{n})_{k,j+1/2}u_{k,j+1/2}^{n+1} & \text{otherwise}\end{cases} \tag{3.32}$$

The mass at the cell interface is defined as the arithmetic average of the masses at the neighbouring cell centres in the momentum equations, $m_{k,j+1/2} = (m_{k,j} + m_{k,j+1})/2$, and the same method is applied to the volume fraction, $\alpha_{k,j+1/2} = (\alpha_{k,j} + \alpha_{k,j+1})/2$.

In the discretised pressure equation (3.19), the continuity equation (3.20), and equation (3.21), the mass flux term, $(mu)_{k,j+1/2}$, at the cell interface, is similarly defined as follows:

$$m_{k,j+1/2}=\begin{cases}m_{k,j} & \text{if } u_{k,j+1/2}>0\\ m_{k,j+1} & \text{otherwise}\end{cases} \tag{3.33}$$

The robustness of the numerical scheme can be strengthened by calculating the fluxes semi-implicitly, which permits violating the CFL condition, in contrast to completely explicit schemes.

3.4.1. System of linear equations

We reorganise all the discretised equations in section 3.3.3, and convert those equations into completely linearised forms. In the programming codes, notation for the cell interface uses a capital letter J instead of $j-1/2$ for computational convenience. The index J counts from 1 to $N+1$, and the cell centre index j counts from 1 to N, where the longitude space is divided into N grid cells.

Gas momentum

$$\begin{aligned}\left(\mathcal{C}_{u,g}^{u_g}\right)_J^n u_{g,J}^{n+1} + \left(\mathcal{C}_{u,g}^{u_g,R}\right)_J^n u_{g,J+1}^{n+1} + \left(\mathcal{C}_{u,g}^{u_g,L}\right)_J^n u_{g,J-1}^{n+1} + \\ + \left(\mathcal{C}_{u,g}^{u_l}\right)_J^n u_{l,J}^{n+1} + \left(\mathcal{C}_{u,g}^{P,R}\right)_J^n P_j^{n+1} + \left(\mathcal{C}_{u,g}^{P,L}\right)_J^n P_{j-1}^{n+1} = (b_{u,g})_J^n\end{aligned} \tag{3.34}$$

Liquid momentum

$$\begin{aligned}\left(\mathcal{C}_{u,l}^{u_l}\right)_J^n u_{l,J}^{n+1} + \left(\mathcal{C}_{u,l}^{u_l,R}\right)_J^n u_{l,J+1}^{n+1} + \left(\mathcal{C}_{u,l}^{u_l,L}\right)_J^n u_{l,J-1}^{n+1} + \\ + \left(\mathcal{C}_{u,l}^{u_g}\right)_J^n u_{g,J}^{n+1} + \left(\mathcal{C}_{u,l}^{P,R}\right)_J^n P_j^{n+1} + \left(\mathcal{C}_{u,l}^{P,L}\right)_J^n P_{j-1}^{n+1} = (b_{u,l})_J^n\end{aligned} \tag{3.35}$$

Pressure equation

$$\begin{aligned}\left(\mathcal{C}_P^P\right)_j^n P_j^{n+1} + \left(\mathcal{C}_P^{u_g,R}\right)_j^n u_{g,J+1}^{n+1} + \left(\mathcal{C}_P^{u_g,L}\right)_j^n u_{g,J}^{n+1} + \\ + \left(\mathcal{C}_P^{u_l,R}\right)_j^n u_{l,J+1}^{n+1} + \left(\mathcal{C}_P^{u_l,L}\right)_j^n u_{l,J}^{n+1} = (b_P)_j^n\end{aligned} \tag{3.36}$$

Gas continuity equation

$$\left(\mathcal{C}_{m,g}\right)_j^n m_{g,j}^{n+1} + \left(\mathcal{C}_{m,g}^R\right)_j^n m_{g,j+1}^{n+1} + \left(\mathcal{C}_{m,g}^L\right)_j^n m_{g,j-1}^{n+1} = (b_{m,g})_{,j}^n \tag{3.37}$$

$$
\mathbf{C}^n = \begin{bmatrix}
\mathcal{C}^{u_g}_{u,g,1} & 0 & & & & & & & & & & \cdots & & & & & & & & & & \cdots \\
0 & \mathcal{C}^{u_l}_{u,l,1} & 0 & & & & & & & & & & & & & & & & & & & \cdots \\
0 & 0 & \mathcal{C}^{P}_{P,1} & 0 & & & & & & & & \cdots & & & & & & & & & & \cdots \\
\vdots & \ddots & \ddots & \ddots & \ddots & & & & & & & \vdots & & & & & & & & & & \vdots \\
\cdots & 0 & \mathcal{C}^{u_g,L}_{P,j-1} & \mathcal{C}^{u_l,L}_{P,j-1} & \mathcal{C}^{P}_{P,j-1} & \mathcal{C}^{u_g,R}_{P,j-1} & \mathcal{C}^{u_l,R}_{P,j-1} & 0 & \mathcal{C}^{P,R}_{P,j-1} & \mathcal{C}^{u_g,R}_{P,j} & \mathcal{C}^{u_l,R}_{P,j} & \cdots & & & & & & & & & & \cdots \\
\cdots & 0 & \mathcal{C}^{u_g,L}_{u,g,J} & 0 & \mathcal{C}^{P,L}_{u,g,J} & \mathcal{C}^{u_g}_{u,g,J} & \mathcal{C}^{u_l}_{u,g,J} & \mathcal{C}^{P,R}_{u,g,J} & \mathcal{C}^{u_g,R}_{u,g,J} & \mathcal{C}^{u_l}_{u,g,J+1} & & 0 & \cdots & & & & & & & & & \cdots \\
\cdots & 0 & 0 & \mathcal{C}^{u_l,L}_{u,l,J} & \mathcal{C}^{P,L}_{u,l,J} & \mathcal{C}^{u_g}_{u,l,J} & \mathcal{C}^{u_l}_{u,l,J} & \mathcal{C}^{P}_{P,j} & \mathcal{C}^{u_g,R}_{P,j} & \mathcal{C}^{u_l,R}_{P,j} & 0 & 0 & \cdots & & & & & & & & & \cdots \\
\cdots & \cdots & \cdots & 0 & 0 & \mathcal{C}^{u_g,L}_{P,j} & \mathcal{C}^{u_l,L}_{P,j} & \mathcal{C}^{P}_{P,j} & \mathcal{C}^{u_g}_{u,g,J+1} & \mathcal{C}^{u_l}_{u,g,J+1} & \mathcal{C}^{P,R}_{u,g,J+1} & \mathcal{C}^{P,R}_{u,l,J+1} & \cdots & & & & & & & & & \cdots \\
\cdots & \cdots & \cdots & \cdots & 0 & \mathcal{C}^{u_g,L}_{u,g,J+1} & 0 & \mathcal{C}^{P,L}_{u,g,J+1} & \mathcal{C}^{u_g}_{u,l,J+1} & \mathcal{C}^{u_l}_{u,l,J+1} & 0 & \mathcal{C}^{P,R}_{u,l,J+1} & \ddots & & & & & & & & & \cdots \\
\cdots & \cdots & \cdots & \cdots & \cdots & 0 & \mathcal{C}^{u_l,L}_{u,l,J+1} & \ddots & \ddots & \ddots & \ddots & \ddots & \ddots & \mathcal{C}^{P}_{P,N} & & & & & & & & \vdots \\
\vdots & \vdots & \vdots & \vdots & \vdots & \vdots & \ddots & & 0 & 0 & 0 & 0 & 0 & \mathcal{C}^{P}_{P,L} & \mathcal{C}^{u_g}_{u,g,N+1} & 0 & & & & & & 0 \\
\cdots & \vdots & \vdots & \vdots & \vdots & \vdots & & & 0 & \mathcal{C}^{u_g,L}_{u,g,N+1} & 0 & 0 & \mathcal{C}^{u_g,L}_{u,g,N+1} & \mathcal{C}^{P,L}_{u,l,N+1} & \mathcal{C}^{u_g}_{u,l,N+1} & \mathcal{C}^{u_l}_{u,g,N+1} & & & & & & \\
\cdots & \cdots & \cdots & \cdots & \cdots & \cdots & \cdots & & \cdots & 0 & \mathcal{C}^{u_l,L}_{u,l,N+1} & \ddots & \ddots & \ddots & \ddots & \mathcal{C}^{u_l}_{u,l,N+1} & & & & & & \\
\end{bmatrix}^n \tag{3.38}
$$

Liquid continuity equation

$$(\mathcal{C}_{m,l})_j^n \, m_{l,j}^{n+1} + \left(\mathcal{C}_{m,l}^R\right)_j^n m_{l,j+1}^{n+1} + \left(\mathcal{C}_{m,l}^L\right)_j^n m_{l,j-1}^{n+1} = (b_{m,l})_{,j}^n \tag{3.39}$$

Pressure equation (3.36), gas momentum equation (3.34), and liquid momentum equation (3.35) are assembled as a system. The system of linear equations is written in the form of $\mathbf{Cx} = \mathbf{b}$, where $\mathbf{C}$ is a coefficient matrix, $\mathbf{x}$ is the unknown vector, and b contains all the residual known terms.

The coefficient matrix $\mathbf{C}$ for the pressure-velocity coupling (a hepta-diagonal matrix) is a sparse banded matrix that can be decomposed into a lower quadrangular matrix and an upper quadrangular matrix using the LU factorisation method (Karris, 2007). Certain elements of the diagonal are highlighted by underlines at the cell j in the matrix in equation (3.38). The coefficients of the mass continuity equations are organised in the similarly as a typical tri-diagonal matrix with a bandwidths of three.

The pressure-velocity coupling gives the following:

$$\mathbf{x}^{n+1} = \begin{bmatrix} u_{g,1} \\ u_{l,1} \\ P_1 \\ \vdots \\ u_{g,J} \\ u_{l,J} \\ P_j \\ \vdots \\ P_N \\ u_{g,N+1} \\ u_{l,N+1} \end{bmatrix}^{n+1} \tag{3.40}$$

The mass for each phase is arranged as follows:

$$\mathbf{x}^{n+1} = \begin{bmatrix} m_{k,1} \\ \vdots \\ m_{k,j-1} \\ m_{k,j} \\ m_{k,j+1} \\ \vdots \\ m_{k,N} \end{bmatrix}^{n+1} \tag{3.41}$$

3.4.2. Non-iterative scheme

The computational sequence for the non-iterative scheme, with a staggered grid structure and the volume error included as a source term when $\dagger = n$. The computational sequence is as follows:

- Assemble and solve the system of linear equations (3.18), (3.17), and (3.19) (pressure-velocity coupling) for P_j^{n+1}, $u_{g,j-1/2}^{n+1}$ and $u_{l,j-1/2}^{n+1}$.
- The mass $m_{k,j}^{n+1}$ is solved for each phase with the updated velocity $u_{k,j-1/2}^{n+1}$.
- The density $\rho_k(P)_j^{n+1}$ is obtained using the state equation with the pressure at the new time level
- The volume error δv can be obtained from equation (3.14).
- Advance to the next time level by one time step.

3.4.3. Iterative scheme

In this scheme, the volume error is excluded from the pressure equation in the inner loop with $\dagger = i$; this error can be included in the computation prior to the inner loop when $\dagger = n$ to accelatrate the convergence rate in some cases. The numerical expression of the compressibility factor, χ_p, is applied rather than the gradient, $\partial\rho_k/\partial P$, in the inner loop, as discussed in section 3.3.1. The computational sequence is:

- Execute the computational procedure of the non-iterative scheme once before continuing the inner loop when $\dagger = n$ (Numerical errors terms are optionally included or not in this step).
- Assemble and solve the system of the linear equations (pressure-velocity coupling) for P_j^i, $u_{g,j-1/2}^i$ and $u_{l,j-1/2}^i$.
- The mass $m_{k,j}^i$ is solved for each phase with the updated velocity $u_{k,j-1/2}^i$.
- The density $\rho_k(P)_j^{n+1}$ is obtained using the state equation with the pressure at the new time level.
- The volume error can be obtained with the updated mass $m_{k,j}^{n+1}$ and the density $\rho_k(P)_j^{n+1}$.
- In the inner loop, the above steps are repeated until the convergence criterion is satisfied, and then the values of the variables $[m_k, u_k, P]^{T,n+1}$ are set equal to $[m_k, u_k, P]^i$. During the inner loop iterations, the fluxes are solved fully implicitly by introducing the values $[m_k, u_k, P]^i$ at $\dagger = i$.
- Advance one time step to the next time level.

3.4.4. Non-staggered liquid velocity

In the temporary work, the upwind method is employed for calculating the semi-implicit fluxes; a similar algorithm is used for the non-iterative scheme in section 3.4.2. In the interfacial friction term, the gas velocity at the cell centre j is calculated by averaging the left and the right states:

$$f_{i,j}^{n}(u_{g,j}^{n+1}-u_{l,j}^{n+1})=f_{i,j}^{n}\left(\frac{1}{2}\left(u_{g,j-1/2}^{n+1}+u_{g,j+1/2}^{n+1}\right)-u_{l,j}^{n+1}\right) \tag{3.42}$$

In the linear part of the friction term $f_{i,j}$, the gas velocity is equal to the right state $u_{g,j+1/2}$ at the jth cell interface when the fluid flows in the positive direction, i.e. $u_{g,j} > 0$, otherwise, the gas velocity is equal to $u_{g,j-1/2}$, if $u_{g,j} < 0$.

3.5. SIMPLE

As a reference scheme to the iterative algorithm, the semi-implicit method of pressure-linked equations (SIMPLE) scheme is briefly introduced in this section, using the discretised equations in Section 3.3.3.

First, the corrected expressions for the pressure and velocities are provided in the literature (Versteeg and Malalasekera, 1995):

$$P = P^{\ddagger}+P^{'} \tag{3.43}$$

$$u_{k,j-1/2} = u_{k,j-1/2}^{\ddagger}+d_{k,j-1/2}\left(P_{j}^{'}-P_{j-1}^{'}\right) \tag{3.44}$$

And the expression of the corrected term d is equal to:

$$d_{k,j-1/2}=\frac{\Delta t}{\Delta x}\alpha_{k,j-1/2}\frac{1}{(\mathcal{C}_{u,k}^{u_k})_{j-1/2}} \tag{3.45}$$

Using the pressure equation (3.19), instead of the continuity equations (Versteeg and Malalasekera, 1995), and substituting equation (3.44) into the pressure

equation, results in:

$$\begin{aligned}
\chi^n_{p,j}P^{'}_j \;+\; & \frac{\Delta t}{\rho^n_{g,j}}\frac{m^{\dagger}_{g,j+1/2}\left[u^{\ddagger}_{g,j+1/2}+d_{g,j+1/2}\left(P^{'}_{j+1}-P^{'}_j\right)\right]}{\Delta x}- \\
- & \frac{\Delta t}{\rho^n_{g,j}}\frac{m^{\dagger}_{g,j-1/2}\left[u^{\ddagger}_{g,j-1/2}+d_{g,j-1/2}\left(P^{'}_{j}-P^{'}_{j-1}\right)\right]}{\Delta x}+ \\
+ & \frac{\Delta t}{\rho^n_{l,j}}\frac{m^{\dagger}_{l,j+1/2}\left[u^{\ddagger}_{l,j+1/2}+d_{l,j+1/2}\left(P^{'}_{j+1}-P^{'}_{j}\right)\right]}{\Delta x}- \\
- & \frac{\Delta t}{\rho^n_{l,j}}\frac{m^{\dagger}_{l,j-1/2}\left[u^{\ddagger}_{l,j-1/2}+d_{l,j-1/2}\left(P^{'}_{j}-P^{'}_{j-1}\right)\right]}{\Delta x}=\delta v^n_j \qquad (3.46)
\end{aligned}$$

Reorganise the above equation (3.46):

$$\begin{aligned}
P^{'}_j\Bigg(\chi^n_{p,j}- & \frac{\Delta t}{\Delta x}\frac{m^{\dagger}_{g,j+1/2}d_{g,j+1/2}}{\rho^n_{g,j}}-\frac{\Delta t}{\Delta x}\frac{m^{\dagger}_{g,j-1/2}d_{g,j-1/2}}{\rho^n_{g,j}}- \\
& -\frac{\Delta t}{\Delta x}\frac{m^{\dagger}_{l,j+1/2}d_{l,j+1/2}}{\rho^n_{l,j}}-\frac{\Delta t}{\Delta x}\frac{m^{\dagger}_{l,j-1/2}d_{l,j-1/2}}{\rho^n_{l,j}}\Bigg)+ \\
& +P^{'}_{j+1}\left(\frac{\Delta t}{\Delta x}\frac{m^{\dagger}_{g,j+1/2}d_{g,j+1/2}}{\rho^n_{g,j}}+\frac{\Delta t}{\Delta x}\frac{m^{\dagger}_{l,j+1/2}d_{l,j+1/2}}{\rho^n_{l,j}}\right)+ \\
& +P^{'}_{j-1}\left(\frac{\Delta t}{\Delta x}\frac{m^{\dagger}_{g,j-1/2}d_{g,j-1/2}}{\rho^n_{g,j}}+\frac{\Delta t}{\Delta x}\frac{m^{\dagger}_{l,j-1/2}d_{l,j-1/2}}{\rho^n_{l,j}}\right) \\
& =\delta v^n_j-\frac{\Delta t}{\Delta x}\frac{m^{\dagger}_{g,j+1/2}u^{\ddagger}_{g,j+1/2}}{\rho^n_{g,j}}+\frac{\Delta t}{\Delta x}\frac{m^{\dagger}_{g,j-1/2}u^{\ddagger}_{g,j-1/2}}{\rho^n_{g,j}} \\
& \quad -\frac{\Delta t}{\Delta x}\frac{m^{\dagger}_{l,j+1/2}u^{\ddagger}_{l,j+1/2}}{\rho^n_{l,j}}+\frac{\Delta t}{\Delta x}\frac{m^{\dagger}_{l,j-1/2}u^{\ddagger}_{l,j-1/2}}{\rho^n_{l,j}} \qquad (3.47)
\end{aligned}$$

Based on the computational sequence presented by Versteeg and Malalasekera, the SIMPLE algorithm is:

- Solve the system of momentum equations (3.17) and (3.18) to obtain $u^{\ddagger}_k$.
- Solve the pressure correction equation (3.47) for the corrected term $P^{'}$.
- Correct the pressure and velocities.

- Solve the mass continuity equations (3.20) and (3.21) for each phase.
- Repeat the above steps until the convergence criterion is satisfied in the inner loop.
- Advance one time step to the next time level.

3.6. Strongly implicit flux splitting method (SIMF-AUSMD)

The method of strongly implicit mixture flux (SIMF) and an advection upstream splitting method (AUSMD), developed by Evje and Flåtten (Evje and Flåtten, 2003, 2005, 2006), are briefly introduced in this section. The SIMF-AUSMD scheme is applied to solve the two-fluid model on a non-staggered arrangement for the coupling of masses and velocities. This algorithm behaves well for stratified flow, which is the primary focus of this work.

With respect to the discretised equations in section 3.3.5, the compressibility factor is:

$$\chi_p = \frac{\alpha_g}{\rho_g}\frac{\partial \rho_g}{\partial p} + \frac{\alpha_l}{\rho_l}\frac{\partial \rho_l}{\partial p} \tag{3.48}$$

The arithmetic average of volume fraction is expressed, as usual:

$$\alpha_{k,j+1/2} = \frac{1}{2}(\alpha_{k,j} + \alpha_{k,j+1}) \tag{3.49}$$

The pressure, at the cell centre j, is computed by the volume balance equation:

$$\frac{m_g}{\rho_g(P)} + \frac{m_l}{\rho_l(P)} = 1 \tag{3.50}$$

The density is a function of the pressure in the equations of state. Because the nonlinear state equations (2.8) and (2.9) are too complex to apply in this scheme, a simpler method is used to obtain the values of $\partial_p \rho_k$ from equations (2.8) and (2.9). The relations of the density and pressure are linearised as follows:

$$\rho_k = \rho_k^0 + \frac{\partial \rho_k}{\partial p}(P - P^0) \tag{3.51}$$

where $P^0 = 1$ bar, $\rho_g^0 = 0.706$ kg/m^3, and $\rho_l^0 = 1000$ kg/m^3 for the cases in this study.

Substituting equation (3.51) into equation (3.50), a quadratic equation with the unknown P is obtained, and the pressure is solved as a positive root of the second-order polynomial.

The convective momentum flux terms in the SIMF scheme are written as follows:

$$(Iu)^*_{k,j+1/2} = U^+_{k,j} I^{n+1}_{k,j} + U^-_{k,j+1} I^{n+1}_{k,j+1} \tag{3.52}$$

The convective mass flux is split into a diffusive flux F^D and a mass flux F^A, associated with the volume fraction calculation. The hybrid mass fluxes F_k (i.e. I^*_k in the continuity equations) are expressed as follows:

$$F_{g,j+1/2} = \frac{1}{\chi_p}\left(\frac{\alpha_g}{\rho_g}\frac{\partial \rho_g}{\partial p} F^D_g + \frac{\alpha_l}{\rho_l}\frac{\partial \rho_l}{\partial p} F^A_g + \frac{\alpha_g}{\rho_l}\frac{\partial \rho_g}{\partial p}(F^D_l - F^A_l)\right) \tag{3.53}$$

and:

$$F_{l,j+1/2} = \frac{1}{\chi_p}\left(\frac{\alpha_l}{\rho_l}\frac{\partial \rho_l}{\partial p} F^D_l + \frac{\alpha_g}{\rho_g}\frac{\partial \rho_g}{\partial p} F^A_l + \frac{\alpha_l}{\rho_g}\frac{\partial \rho_l}{\partial p}(F^D_g - F^A_g)\right) \tag{3.54}$$

The diffusive flux F^D in the SIMF scheme describes the following:

$$F^D_{k,j+1/2} = \frac{1}{2}(I^{n+1}_{k,j} + I^{n+1}_{k,j+1}) + \frac{1}{4}\frac{\Delta x}{\Delta t}(m^{n+1}_{k,j} - m^{n+1}_{k,j+1}) \tag{3.55}$$

and the flux component F^A is as follows:

$$F^A_{k,j+1/2} = U^+_{k,j} m^{n+1}_{k,j} + U^-_{k,j+1} m^{n+1}_{k,j+1} \tag{3.56}$$

Then, $U^{\pm}$ are given as:

$$U^+_{k,j} = \begin{cases} \frac{1}{4c^n_{j+1/2}}(u^n_{k,j} + c^n_{j+1/2})^2 & \text{if } |u^n_{k,j}| < c^n_{j+1/2} \\ \frac{1}{2}(u^n_{k,j} + |u^n_{k,j}|) & \text{otherwise} \end{cases}$$

$$U^-_{k,j+1} = \begin{cases} -\frac{1}{4c^n_{j+1/2}}(u^n_{k,j+1} - c^n_{j+1/2})^2 & \text{if } |u^n_{k,j+1}| < c^n_{j+1/2} \\ \frac{1}{2}(u^n_{k,j+1} - |u^n_{k,j+1}|) & \text{otherwise} \end{cases}$$

Less diffusive formulae for $U^{\pm}$ are employed with the modified coefficient χ_p as described in Evje and Flåtten's articles (Evje and Flåtten, 2005).

The speed of sound at the cell interface is $c_{j+1/2} = max(c_j, c_{j+1})$, and the approximate mixture speed of sound c is defined as:

$$c = \sqrt{\frac{\rho_l \alpha_g + \rho_g \alpha_l}{\partial_p \rho_g \rho_l \alpha_g + \partial_p \rho_l \rho_g \alpha_l}} \tag{3.57}$$

This scheme introduces instability when one phase nearly disappears or occurs in the pipelines. The authors (Evje and Flåtten, 2005) present some

modifications to improve those results in the single-phase region, but the phase appearance and disappearance models are too complex to be incorporated in this numerical formulation. Other feasible methods are employed when only liquid phase exists in a pipe (H. Paillère and Cascales, 2003; Bestion, 2000). This will not be included in the present research work, but it is worthy of study and would be an interesting topic to explore in the future.

3.7. Boundary conditions

The primitive variables $(\alpha_k,\ u_k,\ p)^T$ are preferable as boundary condition to the conservative variables Q. At the inlet of a pipe, all the variables are imposed with specific values; the velocities at the inlet are zero at a closed end. At the outlet boundary, the velocities can be computed by the algorithms in the staggered arrangement (at the cell interface); the values of the velocity, prescribed at the cell centre, are extrapolated from the neighbouring cells. In some scheme, the conservative variable $m_k u_k$ is extrapolated by the known values at neighbouring cell.

In some cases, the liquid cannot flow backward at the outlet. Numerically, the volume fraction of the liquid at the outlet boundary is set equal to zero to ensure this condition.

4. A high-resolution scheme

A two-step MUSCL-Hancock procedure, including a Roe-averaged algorithm, can achieve second-order accuracy. The non-conservative terms in the hyperbolic equations present the most difficulty, arising from the pressure gradient terms and the nonviscous interfacial friction. The primitive variables are stored at the cell centres, and the computational domain is divided into N uniform grid cells. For simplicity, only stratified flow is considered in the present work.

4.1. The FORCE2 scheme: explicit fluxes

Before addressing the Roe-averaged algorithm, a first-order scheme is introduced as a comparison to the high-resolution scheme. The first-order centred with two stages (FORCE2) scheme is added in this section because the same mathematical model, equation (2.5), introduced in section 2.3, is used.

Rewriting equation (3.1) using explicit fluxes and neglecting source terms, the equation for the FORCE2 scheme is developed (Toro, 2006):

$$\mathbf{Q}_j^{n+1} - \mathbf{Q}_j^n + \frac{\Delta t}{\Delta x}\left(\mathbf{F}_{j+1/2}^R - \mathbf{F}_{j-1/2}^L\right) = 0 \tag{4.1}$$

The fluxes are solved by the Lax-Friedrichs (LF) scheme and Richtmyer scheme (Toro, 2006; Munekjord, 2006).

The continuity equations are discretised in a general form:

$$\frac{m_{k,j}^{n+1} - m_{k,j}^n}{\Delta t} + \frac{I_{k,j+1/2} - I_{k,j-1/2}}{\Delta x} = 0 \tag{4.2}$$

The discretised momentum equation for each phase yields the following:

$$\frac{(mu)_{k,j}^{n+1} - (mu)_{k,j}^n}{\Delta t} + \frac{F_{k,j+1/2}^R - F_{k,j-1/2}^L}{\Delta x} = 0 \tag{4.3}$$

4.1.1. Lax-Friedrichs scheme

For mass fluxes, the LF scheme gives the following:

$$I_{k,j+1/2} = \frac{1}{2}\left[(mu)_{k,j}^n + (mu)_{k,j+1}^n\right] + \frac{1}{2}\frac{\Delta x}{\Delta t}\left[m_{k,j}^n - m_{k,j+1}^n\right] \tag{4.4}$$

In the LF scheme, the momentum fluxes can be derived directly from the discretised momentum equation with the simplified expression (2.7) and the simplified nonviscous force for stratified flows. By using central differentiation in the momentum equation, substituting the expression $(mu)^{n+1}$ into equation (4.3), and, sequentially, splitting the resulting equation into two formulae, the right state of interface flux is written as follows:

$$F^R_{k,j+1/2} = F_{k,j+1/2} + \frac{1}{2}\alpha^n_{k,j}\left[P^n_j + P^n_{j+1}\right] \pm \\ \pm \frac{1}{2}\alpha^n_{g,j}\alpha^n_{l,j}\left(u^n_{g,j} - u^n_{l,j}\right)\left(\rho^n_{g,j}\left[u^n_{g,j} + u^n_{g,j+1}\right] + \rho^n_{l,j}\left[u^n_{l,j} + u^n_{l,j+1}\right]\right) \quad (4.5)$$

and the left state of fluxes is written as follows:

$$F^L_{k,j+1/2} = F_{k,j+1/2} + \frac{1}{2}\alpha^n_{k,j+1}\left[P^n_j + P^n_{j+1}\right] \pm \\ \pm \frac{1}{2}\alpha^n_{g,j+1}\alpha^n_{l,j+1}\left(u^n_{g,j+1} - u^n_{l,j+1}\right)\left(\rho^n_{g,j+1}\left[u^n_{g,j} + u^n_{g,j+1}\right] + \right. \\ \left. + \rho^n_{l,j+1}\left[u^n_{l,j} + u^n_{l,j+1}\right]\right) \quad (4.6)$$

apart from the non-conservative terms:

$$F_{k,j+1/2} = \frac{1}{2}\left[\left(mu^2\right)^n_{k,j} + \left(mu^2\right)^n_{k,j+1}\right] + \frac{1}{2}\frac{\Delta x}{\Delta t}\left[(mu)^n_{k,j} - (mu)^n_{k,j+1}\right] \quad (4.7)$$

where the plus sign is for the gas, and minus sign for the liquid phase in equations (4.5) and (4.6).

4.1.2. Richtmyer scheme

There are two stages in this scheme: conserved variables are estimated at the first stage (which can be referred to as the half-time level at $n + 1/2$ or the predictor step in the thesis of Munekjord), and the fluxes are solved at the second stage with values obtained at the first stage.

Deducing the values of m_k and $(mu)_k$ at the cell interface from the discretised mass and momentum equations:

$$m^{n+1/2}_{k,j+1/2} = \frac{1}{2}\left[m^n_j + m^n_{j+1}\right] + \frac{1}{2}\frac{\Delta x}{\Delta t}\left[(mu)^n_j - (mu)^n_{j+1}\right] \quad (4.8)$$

and

$$(mu)^{n+1/2}_{k,j+1/2} = \frac{1}{2}\left[(mu)^n_j + (mu)^n_{j+1}\right] + \frac{1}{2}\frac{\Delta x}{\Delta t}\left[\left(mu^2\right)^n_j - \left(mu^2\right)^n_{j+1}\right] + \\ + \frac{1}{2}\frac{\Delta x}{\Delta t}\alpha^n_{j+1/2}\left[P^n_j - P^n_{j+1}\right] \pm \frac{1}{2}\frac{\Delta x}{\Delta t}\alpha^n_{g,j+1/2}\alpha^n_{l,j+1/2}\left(u^n_{g,j+1/2} - u^n_{l,j+1/2}\right) \\ \left(\rho^n_{g,j+1/2}\left[u^n_{g,j} - u^n_{g,j+1}\right] + \rho^n_{l,j+1/2}\left[u^n_{l,j} - u^n_{l,j+1}\right]\right) \quad (4.9)$$

Solving equations (4.8) and (4.9) leads to the full time level computation with the updated variables at $n + 1/2$ at the second stage (corrector step in the thesis of Munekjord). Then, the mass flux is calculated as follows:

$$I_{k,j+1/2} = (mu)^{n+1/2}_{k,j+1/2} \tag{4.10}$$

The momentum flux of the right state is written as follows:

$$\begin{aligned} F^R_{k,j+1/2} = (mu^2)^{n+1/2}_{k,j+1/2} + \alpha^n_{k,j} P^{n+1/2}_{j+1/2} \pm \\ \pm \frac{1}{2}\alpha^n_{g,j}\alpha^n_{l,j}\left(u^n_{g,j} - u^n_{l,j}\right)\left(\rho^n_{g,j} u^{n+1/2}_{g,j+1/2} + \rho^n_{l,j} u^{n+1/2}_{l,j+1/2}\right) \end{aligned} \tag{4.11}$$

and the left state of the fluxes is written as follows:

$$\begin{aligned} F^L_{k,j+1/2} = (mu^2)^{n+1/2}_{k,j+1/2} + \alpha^n_{k,j+1} P^{n+1/2}_{j+1/2} \pm \\ \pm \frac{1}{2}\alpha^n_{g,j+1}\alpha^n_{l,j+1}\left(u^n_{g,j+1} - u^n_{l,j+1}\right)\left(\rho^n_{g,j+1} u^{n+1/2}_{g,j+1/2} + \rho^n_{l,j+1} u^{n+1/2}_{l,j+1/2}\right) \end{aligned} \tag{4.12}$$

4.1.3. FORCE2

The conservative variables are solved as follows:

$$\mathbf{Q}^{n+1}_j = \mathbf{Q}^n_j - \frac{\Delta t}{\Delta x}\left(\mathbf{F}^R_{j+1/2} - \mathbf{F}^L_{j-1/2}\right) \tag{4.13}$$

The fluxes are formulated as follows:

$$\mathbf{F}_{j+1/2} = \frac{1}{2}\left(\mathbf{F}^{LF}_{j+1/2} + \mathbf{F}^{Rich}_{j+1/2}\right) \tag{4.14}$$

The mass flux I uses equations (4.4) and (4.10). The momentum flux employs the formulae (4.5) and (4.11) as the right state, and the left state of fluxes are presented in equations (4.6) and (4.12).

4.2. Roe-averaged algorithm for the two-phase flow model

Based on the previous work (Kamath and Du, 2009) for a granular-gas model, the existing Roe-averaged algorithm is added to the two-phase flow model containing non-conservative terms. The parameter k is retained in the nonviscous interfacial forces to complete the matrices, and k is equal to 0 for stratified flow (Städtke, 2006).

Reorganising the nonviscous terms in the momentum equations and adding all the non-conservative terms in the flux:

$$\frac{\partial \mathbf{U}}{\partial t} + \frac{\partial \mathsf{F}}{\partial x} = \mathbf{S} \tag{4.15}$$

The primitive variables can be arranged according to the programmer's preference because no specific rules exist. It is prescribed as $\mathbf{V} = [p, u_g, u_l, \alpha_g]^T$ for this application. In this case, the above equation (4.15) is rewritten as follows:

$$\frac{\partial \mathbf{V}}{\partial t} + \frac{d\mathbf{V}}{d\mathbf{U}}\frac{d\mathsf{F}}{d\mathbf{V}}\frac{\partial \mathbf{V}}{\partial x} = \frac{d\mathbf{V}}{d\mathbf{U}}\mathbf{S} \tag{4.16}$$

The Euler-like governing equations, obtained from equation (4.16), are expressed as a function of the conservative variables, $\mathbf{Q}$, as follows:

$$\frac{\partial \mathbf{Q}}{\partial t} + \frac{\partial \mathcal{F}(Q)}{\partial x} + \mathbf{B}^p(Q)\frac{\partial \mathbf{Q}}{\partial x} + \mathbf{B}^{nv}(Q)\frac{\partial \mathbf{Q}}{\partial x} = \mathbf{S}_Q \tag{4.17}$$

The source vector in the above equation is defined as $\mathbf{S}_Q \equiv (d\mathbf{Q}/d\mathbf{U})\mathbf{S}$. The above terms are expanded as follows:

$$\mathbf{Q} = \begin{bmatrix} \alpha_g\rho_g \\ \alpha_l\rho_l \\ \alpha_g\rho_g u_g \\ \alpha_l\rho_l u_l \end{bmatrix} \quad \mathcal{F} = \begin{bmatrix} \alpha_g\rho_g u_g \\ \alpha_l\rho_l u_l \\ \alpha_g\rho_g u_g^2 \\ \alpha_l\rho_l u_l^2 \end{bmatrix} \tag{4.18}$$

The matrix $\mathbf{B}^p$, arising from the pressure gradient term, $\alpha_i \cdot \partial p/\partial x$, is treated as a non-conservative term in the momentum equations; the other non-conservative terms in the matrix, $\mathbf{B}^{nv}$, are introduced by the nonviscous interfacial friction and they can be written in a compact form as $\mathbf{B} = \mathbf{B}^p + \mathbf{B}^{nv}$.

4.2.1. Roe-averaged algorithm

The linearised governing equation is written as follows:

$$\mathbf{Q}_t + \hat{\mathbf{A}}\mathbf{Q}_x + \hat{\mathbf{B}}\mathbf{Q}_x = 0 \tag{4.19}$$

where the Jacobian matrix of the flux vector $\mathbf{A}$ is defined as $\mathbf{A} \equiv d\mathcal{F}/d\mathbf{Q}$ (All the details refer to Appendix B). The expanded form of the matrix A is as follows:

$$\mathbf{A} = \begin{bmatrix} 0 & 0 & 1 & 0 \\ 0 & 0 & 0 & 1 \\ -u_g^2 & 0 & 2u_g & 0 \\ 0 & -u_l^2 & 0 & 2u_l \end{bmatrix} \tag{4.20}$$

The matrix $\mathbf{B}^p$ is written as follows:

$$\mathbf{B}^p = \begin{bmatrix} 0 & 0 & 0 & 0 \\ 0 & 0 & 0 & 0 \\ \alpha_g\rho_l\dfrac{c_0^2}{\rho_s} & \alpha_g\rho_g\dfrac{c_0^2}{\rho_s} & 0 & 0 \\ \alpha_l\rho_l\dfrac{c_0^2}{\rho_s} & \alpha_l\rho_g\dfrac{c_0^2}{\rho_s} & 0 & 0 \end{bmatrix} \tag{4.21}$$

The nonviscous part (Städtke, 2006) is described as:

$$\mathbf{B}^{nv} = \begin{bmatrix} 0 & 0 & 0 & 0 \\ 0 & 0 & 0 & 0 \\ \Delta\alpha_g\rho_l\dfrac{c_0^2}{\rho_s} + \tilde{\alpha}_l u_g \Delta u & \Delta\alpha_g\rho_g\dfrac{c_0^2}{\rho_s} + \tilde{\alpha}_g u_l \Delta u & -\tilde{\alpha}_l\Delta u & -\tilde{\alpha}_g\Delta u \\ \Delta\alpha_l\rho_l\dfrac{c_0^2}{\rho_s} - \tilde{\alpha}_l u_g \Delta u & \Delta\alpha_l\rho_g\dfrac{c_0^2}{\rho_s} - \tilde{\alpha}_g u_l \Delta u & \tilde{\alpha}_l\Delta u & \tilde{\alpha}_g\Delta u \end{bmatrix} \tag{4.22}$$

with

$$c_0^2 = \frac{\alpha_g\rho_l + \alpha_l\rho_g}{\dfrac{\alpha_g\rho_l}{c_g^2} + \dfrac{\alpha_l\rho_g}{c_l^2}} \tag{4.23a}$$

$$\rho_s = \alpha_g\rho_l + \alpha_l\rho_g \tag{4.23b}$$

$$\Delta u = u_g - u_l \tag{4.23c}$$

$$\Delta\alpha_g = \tilde{\alpha}_g - \alpha_g \tag{4.23d}$$

$$\Delta\alpha_l = \tilde{\alpha}_l - \alpha_l \tag{4.23e}$$

where

$$\tilde{\alpha}_g = \frac{\alpha_g\rho_g\left[\rho_l + k(\alpha_g\rho_g + \alpha_l\rho_l)\right]}{\rho_g\rho_l + k(\alpha_g\rho_g + \alpha_l\rho_l)^2} \tag{4.24}$$

$$\tilde{\alpha}_l = \frac{\alpha_l\rho_l(\rho_g + k\left[\alpha_g\rho_g + \alpha_l\rho_l\right])}{\rho_g\rho_l + k(\alpha_g\rho_g + \alpha_l\rho_l)^2} \tag{4.25}$$

The equations obey the laws of conservation of volume.

$$\tilde{\alpha}_g + \tilde{\alpha}_l = 1 \tag{4.26}$$

For the stratified flow, $k = 0$, and $\tilde{\alpha}_g$ and $\tilde{\alpha}_l$ are reduced to α_g and α_l, respectively.

The matrices $\hat{\mathbf{A}}$ and $\hat{\mathbf{B}}$, are evaluated at the Roe-averaged states, and the eigenvalues and their corresponding eigenvectors (the matrix of right eigenvectors R and its inverse matrix R^{-1}) of the matrix $\mathbf{A}+\mathbf{B}$, can be solved:

$$\lambda_1 = u_g;\ \lambda_2 = u_l;\ \lambda_3 = u_s + c;\ \lambda_4 = u_s - c \tag{4.27}$$

The mixture velocity u_s and mixture speed of sound c are expressed as follows:

$$u_s = \frac{\rho_g\rho_l\left(\alpha_g u_g + \alpha_l u_l\right) + k\left(\alpha_g\rho_g + \alpha_l\rho_l\right)\left(\alpha_g\rho_g u_g + \alpha_l\rho_l u_l\right)}{\rho_g\rho_l + k(\alpha_g\rho_g + \alpha_l\rho_l)^2} \tag{4.28}$$

and

$$c^2 = \mathcal{C}_0^2 - \Delta\mathcal{U}^2 \tag{4.29}$$

where

$$\mathcal{C}_0^2 = \frac{\alpha_g\rho_l + \alpha_l\rho_g}{\dfrac{\alpha_g\rho_l}{c_g^2} + \dfrac{\alpha_l\rho_g}{c_l^2}} \frac{1 + k\dfrac{\alpha_g\rho_g + \alpha_l\rho_l}{\alpha_g\rho_l + \alpha_l\rho_g}}{1 + k\dfrac{\alpha_g\rho_g + \alpha_l\rho_l}{\rho_g\rho_l}} \tag{4.30}$$

and

$$\Delta\mathcal{U}^2 = \alpha_g\alpha_l\rho_g\rho_l\left(u_g - u_l\right)^2 \frac{\left[\rho_g + k\left(\alpha_g\rho_g + \alpha_l\rho_l\right)\right]\left[\rho_l + k\left(\alpha_g\rho_g + \alpha_l\rho_l\right)\right]}{\left[\rho_g\rho_l + k\left(\alpha_g\rho_g + \alpha_l\rho_l\right)^2\right]^2} \tag{4.31}$$

The Rankine-Hugoniot jump condition should be obeyed across the isolated discontinuities with velocity $s(x,t)$ (Kamath and Du, 2009):

$$s(\mathbf{Q}_R - \mathbf{Q}_L) = \mathcal{F}(Q_R) - \mathcal{F}(Q_L) + \frac{1}{2}\left[\mathbf{B}(Q_R) + \mathbf{B}(Q_L)\right](\mathbf{Q}_R - \mathbf{Q}_L) \tag{4.32}$$

In the above formula, the matrix $\mathbf{B}(Q)$ arising from the non-conservative terms should be bounded in a sufficiently small neighbourhood. In the linearised governing equations, the wave propagation speed s is the eigenvalue of the matrix $\hat{\mathbf{A}} + \hat{\mathbf{B}}$:

$$(\hat{\mathbf{A}} + \hat{\mathbf{B}})(\mathbf{Q}_R - \mathbf{Q}_L) = \mathcal{F}(Q_R) - \mathcal{F}(Q_L) + \frac{1}{2}\left[\mathbf{B}(Q_R) + \mathbf{B}(Q_L)\right](\mathbf{Q}_R - \mathbf{Q}_L) \tag{4.33}$$

The above equation can be split into two expressions, one of which is the balance equation of the non-conservative terms:

$$\hat{\mathbf{A}}(Q_R - Q_L) = \mathcal{F}(Q_R) - \mathcal{F}(Q_L) \tag{4.34}$$

$$\hat{\mathbf{B}}(Q_R - Q_L) = \frac{1}{2}\left[\mathbf{B}(Q_R) + \mathbf{B}(Q_L)\right](\mathbf{Q}_R - \mathbf{Q}_L) \tag{4.35}$$

The Roe-averaged states can be determined by the above conditions for consistency. In addition, the variables $\hat{\alpha}$, $\hat{\rho}$, and $\hat{u}$ should be determined accordingly for each phase. The roe-averaged $\hat{u}$ can be solved directly from equation (4.34):

$$\hat{u} = \frac{\sqrt{\alpha_L \rho_L} u_L + \sqrt{\alpha_R \rho_R} u_R}{\sqrt{\alpha_L \rho_L} + \sqrt{\alpha_R \rho_R}} \tag{4.36}$$

For the consistency of equation $d(\alpha\rho u) = \widehat{\alpha\rho} du + \hat{u} d(\alpha\rho)$, the following average should be obeyed:

$$\widehat{\alpha\rho} = \sqrt{\alpha_R \rho_R} \cdot \sqrt{\alpha_L \rho_L} \tag{4.37}$$

The influence of the average $\widehat{\alpha\rho}$ can be neglected with no loss in the accuracy of results with the forms of averages $\hat{\alpha}$ and $\hat{\rho}$. One way is defined by Munekjord:

$$\hat{\alpha} = \frac{\alpha_L + \alpha_R}{2} \tag{4.38}$$

$$\hat{\rho} = \frac{\rho_L + \rho_R}{2} \tag{4.39}$$

Equation $d(\alpha\rho) = \hat{\alpha} d\rho + \hat{\rho} d\alpha$ is established by substituting the above averages, but these averages contrast with equation (4.37). Hence, the variables $\hat{\alpha}$ and $\hat{\rho}$ can also be prescribed by equation (4.37):

$$\hat{\alpha} = \sqrt{\alpha_L \alpha_R} \tag{4.40}$$

$$\hat{\rho} = \sqrt{\rho_L \rho_R} \tag{4.41}$$

The average $\widehat{(d\rho/dp)}$ is obtained:

$$\widehat{\left(\frac{d\rho}{dp}\right)} = \begin{cases} \dfrac{\rho_R - \rho_L}{p_R - p_L} & \text{if} \quad p_R \neq p_L \\ \dfrac{\partial \rho}{\partial p} & \text{otherwise} \end{cases} \tag{4.42}$$

Equation (4.33) can be decomposed as follows:

$$\hat{\mathbf{R}} \hat{\mathbf{\Lambda}^+} \hat{\mathbf{R}}^{-1} = \mathcal{F}(Q_R) - \mathbf{F}_I(Q_l, Q_R) + \hat{\mathbf{B}}^{nv} \mathbf{Q}_R + \frac{1}{2} \mathbf{B}^p(Q_R)(\mathbf{Q}_R - \mathbf{Q}_L) \tag{4.43}$$

$$\hat{\mathbf{R}} \hat{\mathbf{\Lambda}^-} \hat{\mathbf{R}}^{-1} = \mathcal{F}(Q_L) + \mathbf{F}_I(Q_l, Q_R) - \hat{\mathbf{B}}^{nv} \mathbf{Q}_L + \frac{1}{2} \mathbf{B}^p(Q_L)(\mathbf{Q}_R - \mathbf{Q}_L) \tag{4.44}$$

and $\hat{\mathbf{\Lambda}^{\pm}}$ is the diagonal matrix of eigenvalues that can be decomposed into a positive matrix $\mathbf{\Lambda}^+$ and a negative one $\mathbf{\Lambda}^-$.

For the nonviscous part of equation (4.35), the expression $\hat{\mathbf{B}}^{nv}(\mathbf{Q}_R - \mathbf{Q}_L)$ is submitted in the above decomposition. In the matrix $\mathbf{B}^p$, the approximate

integral $\frac{1}{2}\left[\mathbf{B}^p(Q_R)+\mathbf{B}^p(Q_L)\right](\mathbf{Q}_R-\mathbf{Q}_L)$ in equation (4.35) is implemented in the formula of the interface fluxes.

The interface flux, $\mathbf{F}_I(Q_L,Q_R)$, is found by solving equations (4.43) and (4.44):

$$\mathbf{F}_I(Q_L,Q_R)=\frac{1}{2}\left[\mathcal{F}(Q_L)+\mathcal{F}(Q_R)+\left[\mathbf{B}^p(Q_R)-\mathbf{B}^p(Q_L)\right](\mathbf{Q}_R-\mathbf{Q}_L)\right.$$
$$\left.+\hat{\mathbf{B}}^{nv}(\mathbf{Q}_L+\mathbf{Q}_R)\right]-\frac{1}{2}\left(\hat{\mathbf{R}}|\hat{\wedge}|\hat{\mathbf{R}}^{-1}(\mathbf{Q}_R-\mathbf{Q}_L)\right) \quad (4.45)$$

The Roe-averaged state $\hat{\mathbf{Q}}=\mathbf{Q}(Q_L,Q_R)$ is a function of the left and right states. The left and right states of the primitive variables in the above equations are solved using the limited gradients, $\mathbf{V}_x$, that are obtained with the min-mod limiter:

$$\mathbf{V}_x=\frac{1}{\Delta x}\Phi(\Delta_+\mathbf{V},\Delta_-\mathbf{V}) \quad (4.46)$$

and Φ is a limiting function of the associated forward (Δ_+V) and backward (Δ_-V) difference with the limiting performed on the primitive variables for simplicity:

$$(\mathbf{V}_L)_{j+1/2} = \mathbf{V}_j+\frac{\Delta x}{2}(\mathbf{V}_x)_j \quad (4.47)$$

$$(\mathbf{V}_R)_{j+1/2} = \mathbf{V}_{j+1}-\frac{\Delta x}{2}(\mathbf{V}_x)_{j+1} \quad (4.48)$$

More details, related to the Roe-averaged algorithm, can be found in Appendix D.

4.2.2. The MUSCL-Hancock procedure

Using the two-step MUSCL-Hancock procedure, the two-phase flow model can be solved with high resolution by performing the Roe-averaged algorithm. In the first step, the derivatives of conservative variables with respect to time at computational cell j are expressed as follows:

$$(\mathbf{Q}_t)_j^n=-\frac{\mathcal{F}_{j+1/2}^n-\mathcal{F}_{j-1/2}^n}{\Delta x}-\frac{\mathbf{B}_{j+1/2}^n}{2}\frac{\mathbf{Q}_{j+1}^n-\mathbf{Q}_j^n}{\Delta x}-\frac{\mathbf{B}_{j-1/2}^n}{2}\frac{\mathbf{Q}_j^n-\mathbf{Q}_{j-1}^n}{\Delta x}+\mathbf{S}_Q^n \quad (4.49)$$

Then, the values of the primitive variables at the half-time level are updated:

$$\mathbf{V}(x,t)=\mathbf{V}_j^n+(x-x_j)(\mathbf{V}_x)_j^n+(t-t^n)(\mathbf{V}_t)_j^n \quad (4.50)$$

with $x_{j-1/2}\leqslant x\leqslant x_{j+1/2}$ and $t^n\leqslant t\leqslant t^{n+1}$, where $(\mathbf{V}_t)_j^n=(d\mathbf{V}/d\mathbf{Q})_j^n(\mathbf{Q}_t)_j^n$ and $(\mathbf{Q}_t)_j^n$ are obtained from equation (4.49).

The second step is as follows:

$$\frac{\mathbf{Q}_j^{n+1} - \mathbf{Q}_j^n}{\Delta t} = (\mathbf{Q}_t)_j^{n+1/2} \tag{4.51}$$

4.3. Boundary conditions

The primitive variables, $\mathbf{V}$, are established at boundaries by imposing certain values or by linearly extrapolating the known values at the correspondingly neighbouring cells.

5. Numerical Issues

Three numerical issues are presented in this chapter. Through the comparison of the numerical results, the profiles are analysed by capturing two-phase flows in pipes: stratified flow is the primary focus, and the severe slugging type of flow is investigated in one example.

5.1. Iterative versus non-iterative schemes

In this section, cases are tested to quantify advantages of the inner loop iteration. The goal is to determine if the iterative scheme improves the accuracy without costing unbearable computational effort compared to the non-iterative scheme. Articles 1 and 2 show the numerical results predicted by the two schemes, and an analysis of the comparison indicates that the non-iterative scheme is more efficient, the iterative scheme exihibits an advantage in the accuracy (however, not very great), and the iterative scheme consumes many times more computational time and greater effort contributed by numerators than the non-iterative scheme.

In this numerical issue, thermal cases are tested. And a sub-issue, where the energy balance equation can be involved in the computation simultaneously or sequentially, is discussed. The simultaneous scheme is more accurate and it is described in Article 2.

5.2. Staggered versus non-staggered schemes

The non-staggered schemes avoid the false phenomena caused by the staggered grid arrangement. The SIMF-AUSMD (Evje and Flåtten, 2006) method is more accurate than the other two schemes with an efficiency similar to a single precision method; the staggered semi-implicit upwind method (SSUM) is the most robust scheme studied in this work. More specifically, the SSUM scheme is stable even when the pipeline is completely filled by the liquid, while the other schemes are unreliable in this situation, e.g. the volume fraction of water exceeds 0.8 at the lower section of the pipe. For more details, refer to the

corresponding Article 3.

5.3. Second-order versus first-order schemes

As discussed in Chapter 4, the Roe-averaged algorithm and the FORCE2 scheme are compared for numerical accuracy.

5.3.1. Large relative velocity shock tube

The initial values (Evje and Flåtten, 2003) in this large relative velocity shock tube test case are as follows:

$$V_L = \begin{bmatrix} p \\ u_g \\ u_l \\ \alpha_g \end{bmatrix} = \begin{bmatrix} 265000\,\text{Pa} \\ 65\,\text{m/s} \\ 1\,\text{m/s} \\ 0.29 \end{bmatrix} \tag{5.1}$$

$$V_R = \begin{bmatrix} p \\ u_g \\ u_l \\ \alpha_g \end{bmatrix} = \begin{bmatrix} 265000\,\text{Pa} \\ 50\,\text{m/s} \\ 1\,\text{m/s} \\ 0.3 \end{bmatrix} \tag{5.2}$$

The length is 100 m and the initial discontinuity is located at 50 m. The domain is divided into 1000 computational grid cells with a time step of 10^{-4} s.

The comparison between the Roe-averaged algorithm and the FORCE2 scheme is shown in Figures 5.1 and 5.2.

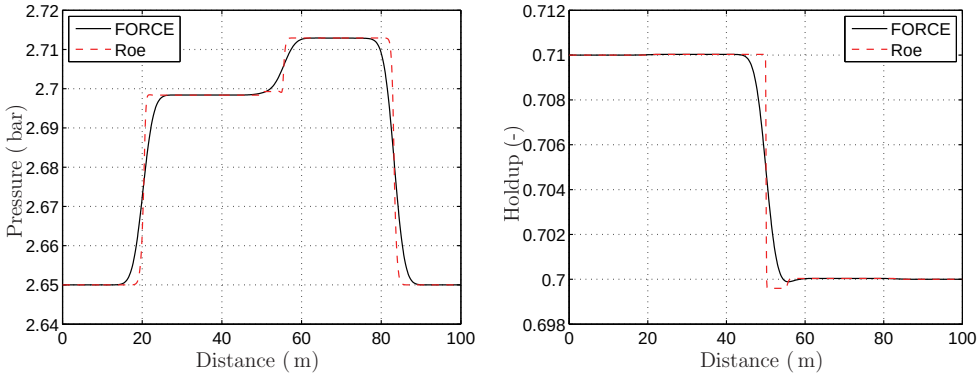

Figure 5.1.: *Large relative velocity shock tube at* 0.1 s

The Roe-averaged algorithm completely achieves second-order precision in contrast to the FORCE2 scheme. The capability has been demonstrated by capturing shocks. The non-conservative terms are consistently incorporated with the conservative flux terms in the flux formula.

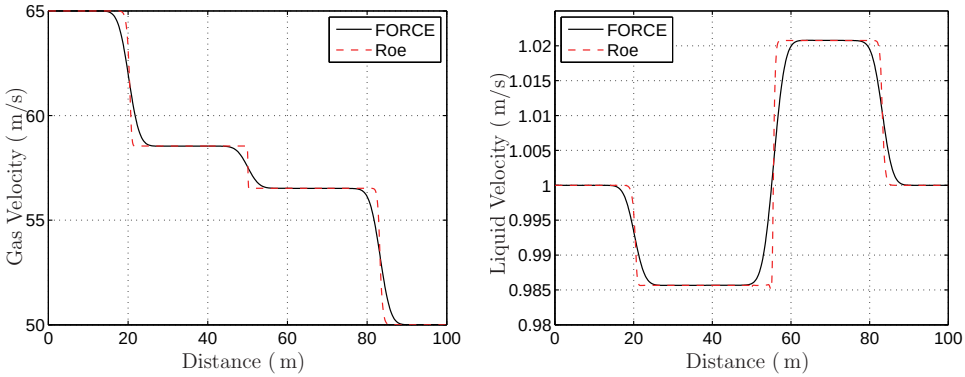

Figure 5.2.: *Phase velocities in large relative velocity shock tube at* 0.1 s

6. Remarks

When the advantages and disadvantages of a numerical scheme are discussed, the intention is always to assess its robustness, computational efficiency, and accuracy. This short summary will thus focus on these aspects.

6.1. Robustness

Based on the test cases, the staggered semi-implicit upwind method receives five stars for robustness. The semi-implicit schemes are more stable than the other schemes tested because of the allowance for the violation of the CFL criterion. Even though this method is diffusive with a coarse grid, its robustness cannot be matched by the other numerical schemes used in this work.

6.2. Computational efficiency

The non-iterative schemes, certainly, are more efficient than the schemes that include inner loops; the high-resolution algorithm requires more computational time in contrast to the first-order numerical schemes. Despite the computational ability of computers has been greatly increased in the recent years computational time is still an obstacle in the field of CFD. Even if one day computer technology shall advance to a point that the computation time becomes less critical, the staggered semi-implicit upwind method can still be implemented as a robust and efficient rehearsal for the formal simulations to predict the profiles of fluid flow properties without redundant effort in programming and numerics.

6.3. Accuracy

The flux-splitting method is more accurate than the staggered upwind method. The second-order precision scheme has the advantage of finer computed resolution. This level of computational accuracy is not normally required in most large scale pipelines utilised in the industry. However, in some small

scale applications, the computational accuracy is necessary to help engineers understand the physics better.

Bibliography

Bergant, A., A. Sompson, and A. Tijsseling (2006). Water hammer with column separation: A historical review. *Journal of Fluids and Structure 22*, 135–171.

Bestion, D. (2000, September). The phase appearance and disappearance in the cathare code. In *Trends in Numerical and Physical Modeling for Industrial Multiphase Flows*, Cargese, France.

Boris, J. P. and D. L. Book (1997). Flux-corrected transport. *Journal of Computational Physics 135*, 172–186.

Brunone, B., B. W. Karney, M. Mecarelli, and M. Ferrante (2000). Velocity profiles and unsteady pipe friction in transient flow. *Journal of water Resources Planning and Mangement 126*(4), 236–244.

Chen, S. and G. D. Doolen (1998). Lattice boltzmann method for fluid flows. *Fluid Mechanics 30*, 329–364.

Drew, D., I. Cheng, and R. T. Drew (1979). The analysis of virtual mass effects in two-phase flow. *International Journal fo Multiphase Flow 5*, 233–242.

Evje, S. and T. Flåtten (2003). Hybrid flux-splitting schemes for a common two-fluid model. *Journal of Computational Physics 192*, 175–210.

Evje, S. and T. Flåtten (2005). Weakly implicit numerical schemes for a two-fluid model. *SIAM. Joural on Scitific Computing 26*, 1449–1484.

Evje, S. and T. Flåtten (2006). CFL-violating numerical schemes for a two-fluid model. *Journal of Scientific Computing 29*, 83–114.

Ferziger, J. H. and M. Peric (2002). *Computational Methods for Fluid Dynamic*. Springer.

Flåtten, T. (2003). *Hybrid flux splitting schemes for numerical resolution of two-phase flows*. Ph. D. thesis, Norwegian University of Science and Technology, Trondheim, Norway.

H. Paillère, C. C. and J. G. Cascales (2003). On the extension of the ausm+ scheme to compressible two-fluid models. *Computers and Fluids 32*, 891–916.

Henau, V. D. (1992). *A Study of Terrain-Induced Slugging in Two-phase Flow Pipelines*. Ph. D. thesis, University of Waterloo.

Ishii, M. and T. Hibiki (2006). *Thermo-Fluid Dynamics of Two-Phase Flow*. Springer.

Kamath, H. and X. Du (2009). A roe-average algorithm for a granular-gas model with non-conservative terms. *Journal of Computational Physics 228*, 8187–8202.

Karris, S. T. (2007). *Numerical Analysis Using MATLAB and Excel*. Orchard Publications.

Khamlichi, A., L. Jezequel, and F. Tephany (1995). Elastic-plastic water hammer analysis in piping systems. *Wave Motion 22*, 279–295.

LeVeque, R. J. (2002). *Finite-Volume Methods for Hyperbolic Problems*. Cambridge University Press.

Li, Q. S., K. Yang, and L. Li (2003). Analytical solution for fluid-structure interaction in liquid-filled pipe subjected to impact-induced water hammer. *Journal of Engineering Mechanics 129*(22), 1408.

Liou, M. S. (1996). A sequel to ausm: Ausm+. *Journal of Computational Physics 129*, 364–382.

Mohamed, S. G., S. G. S. Mansour, and M. Zhao (2002). Applicability of quasisteady and axisymmetric turbulence models in water hammer. *Journal of Hydraulic Engineering 128*.

Munekjord, S. T. (2006). *Analysis of The Two-Fluid Model And The Drift-Flux Model for Numerical Calculation of Two-Phase Flow*. Ph. D. thesis, Norwegian University of Science and Technology, Trondheim, Norway.

Novotny, A. and I. Straskraba (2004). *Introduction to the Mathematical Theory of Compressible Flow*. Oxford University Press.

Pezzinga, G. (1999). Quasi-2d model for unsteady flow in pipe network. *Journal of Hydraulic Engineering 125*(7), 676–685.

Pezzinga, G. (2000). Evalution of unsteady flow resistances by quasi-2d or 1d models. *Journal of Hydraulic Engineering 126*(10), 778–785.

Pezzinga, G. and P. Scandura (1995). Unsteady flow in institutions with polymeric additional pipe. *Journal of Hydraulic Engineering 121*(11), 802–811.

Prausnitz, J. M., R. N. Lichtenthaler, and E. G. Azevedo (1999). *Molecular Thermodynamics of Fluid-Phase Equilibria*. Prentice-Hall PTR.

Prosperetti, A. and G. Tryggvason (2009). *Computational Methods for Multiphase Flow*. Cambridge University Press.

Shin, Y. W. and W. L. Chen (1975). Numrical fluid-hammer analysis by the method of characteristics in complex piping networks. *Nuclear Engineering and Design 33*, 357–369.

Städtke, H. (2006). *Gasdynamic Aspects of Two-Phase Flow: Hyperbolicity,*

Wave Propagation Phenomena, and Related Numerical Methods. WILEY-VCH.

Taitel, Y. (1986). Stability of severe slugging. *International Journal of Multiphase Flowt 12*, 203–217.

The Engineering ToolBox, W. (2008). Density of fluids - changing pressure and temperature, and 'howpublished'. `http://www.engineeringtoolbox.com/fluid-density-temperature-pressure-d_309.html`.

Toro, E. F. (2006). Musta: A multi-stage numerical flux. *Applied Numerical Mathematics 56*, 1464–1479.

Versteeg, H. K. and W. Malalasekera (1995). *An Introduction to Computational Fluid Dynamics: The Finite Volume Method.* Pearson, Prentice Hall.

A. Friction forces

In single-phase flow, the friction force is expressed in a simple way as $f_w u = -\lambda\rho\,|u|\,u/2D$, where λ is the friction factor and D is the pipe diameter. The friction factor λ is an empirical constant associated with different flow regimes.

Similarly, the friction force $f_k u_k$ equals to $-\lambda_k \alpha_k \rho_k\,|u_k|\,u_k/2D$ in two-phase flow.

Then, the interfacial friction F_g^{int} can be written as follows:

$$F_g^{int} = f_g^{int}(u_g - u_l) = -\frac{1}{2D}\alpha_l \rho_g \lambda_i\,|u_g - u_l|\,(u_g - u_l) \tag{A.1}$$

$$F_l^{int} = -F_g^{int} \tag{A.2}$$

The interfacial friction factor λ_i is normally given as an empirical value.

B. The LU factorisation

To understand this method, an example with a simple matrix is used. In the pressure-velocity coupling system of the single-phase flow model, the coefficients matrix $\mathbf{C}$ is a penta-diagonal with two super-diagonals and two sub-diagonals that can be decomposed into a lower triangular matrix $\mathbf{C}^{lower}$ and an upper triangular matrix $\mathbf{C}^{upper}$ (Karris, 2007).

Simply, the linearised equations are written as a system:

$$\mathbf{C} \cdot \mathbf{x} = \mathbf{b} \tag{B.1}$$

and the matrix $\mathbf{C}$ is split into $\mathbf{C}^{lower}$ and $\mathbf{C}^{upper}$. Then, we have the following:

$$\mathbf{C}^{lower} \cdot \mathbf{C}^{upper} \cdot \mathbf{x} = \mathbf{b} \tag{B.2}$$

It is assumed that $\mathbf{y} = \mathbf{C}^{upper} \cdot \mathbf{x}$, and the following equation is solved:

$$\mathbf{C}^{lower} \cdot \mathbf{y} = \mathbf{b} \tag{B.3}$$

The variables are then obtained:

$$\mathbf{C}^{upper} \cdot \mathbf{x} = \mathbf{y} \tag{B.4}$$

The method itself is not complex, but the size of the coefficients matrix often increases the computational effort, requiring patience to program the codes. Other methods can be considered instead of the LU factorisation, but the present method is more efficient compared to the two other methods introduced in the textbook written by Karris.

C. Nonviscous interfacial forces for hyperbolic two-phase flow model

As depicted in the literature, there are three contributions in the nonviscous part of the interfacial force, F_k^{int}, with some postulations (Städtke, 2006):

$$F_g^{nv} = F_g^{vm} + F_g^{\Delta p} + F_g^{comp} \tag{C.1}$$

The virtual mass force formula suggested by Drew et al. can be written as follows:

$$F_g^{vm} = \rho_l C_{vm} \left[\left(\frac{\partial u_g}{\partial t} - \frac{\partial u_l}{\partial t} + u_l \frac{\partial u_g}{\partial x} - u_g \frac{\partial u_l}{\partial x} \right) + (\lambda - 1)(u_g - u_l) \left(\frac{\partial u_g}{\partial x} - \frac{\partial u_l}{\partial x} \right) \right] \tag{C.2}$$

where the parameters C_{vm} and λ are dependent on the gas volume fraction α_g. It is found that the value of C_{vm} varies according to the shapes of the particles (Drew et al., 1979); the parameter λ should be determined by an empirical test. The following form is proposed by Städtke:

$$F_g^{vm} = -\alpha_g \alpha_l (\alpha_g \rho_g + \alpha_l \rho_l) \left[k \left(\frac{\partial u_g}{\partial t} - \frac{\partial u_l}{\partial t} + u_l \frac{\partial u_g}{\partial x} - u_g \frac{\partial u_l}{\partial x} \right) + d(u_g - u_l) \left(\frac{\partial u_g}{\partial x} - \frac{\partial u_l}{\partial x} \right) \right] \tag{C.3}$$

The compressibility effect contributes to the form:

$$F_g^{comp} = -\alpha_g \alpha_l (u_g - u_l) \left[r_g \left(\frac{\partial \rho_g}{\partial t} + u_g \frac{\partial \rho_g}{\partial x} \right) + r_l \left(\frac{\partial \rho_l}{\partial t} + u_l \frac{\partial \rho_l}{\partial x} \right) \right] \tag{C.4}$$

The pressure difference between phase and interface influences the interfacial forces as follows:

$$F_g^{\Delta p} = -\alpha_g \alpha_l (\alpha_g \rho_g + \alpha_l \rho_l) e (u_g - u_l)^2 \frac{\partial \alpha_g}{\partial x} \tag{C.5}$$

The parameters d, r_g, r_l, and e are obtained on the basis of the eigen-structure and physical meanings simultaneously (Städtke, 2006):

$$\begin{aligned} d &= \frac{\alpha_l\rho_g - \alpha_g\rho_l}{\alpha_g\rho_g + \alpha_l\rho_l} \\ r_g &= \frac{\alpha_g(\rho_g + \rho_l)}{\rho_g} \\ r_l &= \frac{\alpha_l(\rho_g + \rho_l)}{\rho_l} \\ e &= \frac{\rho_g + \rho_l}{\alpha_g\rho_g + \alpha_l\rho_l} \end{aligned} \tag{C.6}$$

D. Roe-averaged algorithm

D.1. Pressure gradient

An additional way to solve the pressure gradient term is recommended by Städtke:

$$\alpha_g \frac{\partial p}{\partial x} = \frac{\partial \alpha_g p}{\partial x} - p\frac{\partial \alpha_g}{\partial x} \tag{D.1}$$

The conservative flux becomes the following:

$$\mathcal{F} = \begin{bmatrix} \alpha_g \rho_g u_g \\ \alpha_l \rho_l u_l \\ \alpha_g \rho_g u_g^2 + \alpha_g p \\ \alpha_l \rho_l u_l^2 + \alpha_l p \end{bmatrix} \tag{D.2}$$

Then, the matrix $\mathbf{A}$ and the matrix $\mathbf{B}$ can be rewritten as follows:

$$\mathbf{A} = \begin{bmatrix} 0 & 0 & 1 & 0 \\ 0 & 0 & 0 & 1 \\ \alpha_g \rho_l \frac{c_0^2}{\rho_s} + p\frac{\alpha_l}{c_l^2}\frac{c_0^2}{\rho_s} - u_g^2 & \alpha_g \rho_g \frac{c_0^2}{\rho_s} - p\frac{\alpha_g}{c_g^2}\frac{c_0^2}{\rho_s} & 2u_g & 0 \\ \alpha_l \rho_l \frac{c_0^2}{\rho_s} - p\frac{\alpha_l}{c_l^2}\frac{c_0^2}{\rho_s} & \alpha_l \rho_g \frac{c_0^2}{\rho_s} + p\frac{\alpha_g}{c_g^2}\frac{c_0^2}{\rho_s} - u_l^2 & 0 & 2u_l \end{bmatrix} \tag{D.3}$$

The matrix $\mathbf{B}^p$ is used as follows:

$$\mathbf{B}^p = \begin{bmatrix} 0 & 0 & 0 & 0 \\ 0 & 0 & 0 & 0 \\ -p\frac{\alpha_l}{c_l^2}\frac{c_0^2}{\rho_s} & p\frac{\alpha_g}{c_g^2}\frac{c_0^2}{\rho_s} & 0 & 0 \\ p\frac{\alpha_l}{c_l^2}\frac{c_0^2}{\rho_s} & -p\frac{\alpha_g}{c_g^2}\frac{c_0^2}{\rho_s} & 0 & 0 \end{bmatrix} \tag{D.4}$$

The non-viscous part is written as:

$$\mathbf{B}^{nv} = \begin{bmatrix} 0 & 0 & 0 & 0 \\ 0 & 0 & 0 & 0 \\ \Delta\alpha_g\rho_l\dfrac{c_0^2}{\rho_s} + \tilde{\alpha}_l u_g \Delta u & \Delta\alpha_g\rho_g\dfrac{c_0^2}{\rho_s} + \tilde{\alpha}_g u_l \Delta u & -\tilde{\alpha}_l\Delta u & -\tilde{\alpha}_g\Delta u \\ \Delta\alpha_l\rho_l\dfrac{c_0^2}{\rho_s} - \tilde{\alpha}_l u_g \Delta u & \Delta\alpha_l\rho_g\dfrac{c_0^2}{\rho_s} - \tilde{\alpha}_g u_l \Delta u & \tilde{\alpha}_l\Delta u & \tilde{\alpha}_g\Delta u \end{bmatrix} \tag{D.5}$$

The interface flux formula (4.45) and $\mathbf{B}^p$ can be solved either in this way or as mentioned in section 4.2.1.

D.2. Coefficient matrices for the Roe-averaged algorithm

Recalling equation (4.15) in section 4.2.1:

$$\frac{\partial \mathbf{U}}{\partial t} + \frac{\partial \mathsf{F}}{\partial x} = \mathbf{S} \tag{D.6}$$

The expanded terms are as follows:

$$\mathbf{U} = \begin{bmatrix} \alpha_g\rho_g \\ \alpha_l\rho_l \\ \alpha_g\rho_g u_g + \bar{\chi}^{vm} k\,(u_g - u_l) + \bar{\chi}_t^p p \\ \alpha_l\rho_l u_l - \bar{\chi}^{vm} k\,(u_g - u_l) - \bar{\chi}_t^p p \end{bmatrix} \tag{D.7}$$

with

$$\bar{\chi}^{vm} = \bar{\alpha}_g\bar{\alpha}_l(\bar{\alpha}_g\bar{\rho}_g + \bar{\alpha}_l\bar{\rho}_l) \tag{D.8}$$

$$\bar{\chi}_t^p = \bar{\alpha}_g\bar{\alpha}_l(\bar{\rho}_g + \bar{\rho}_l)(\bar{u}_g - \bar{u}_l)\frac{1}{\bar{\rho}_g\bar{\rho}_l}\frac{\bar{\rho}_s}{\bar{c}_0^2} \tag{D.9}$$

F including the non-viscous part can be written as follows:

$$\mathsf{F} = \begin{bmatrix} \alpha_g\rho_g u_g \\ \alpha_l\rho_l u_l \\ \alpha_g\rho_g u_g^2 + \bar{\alpha}_g p + \bar{\chi}^{vm} k(\bar{u}_l u_g - \bar{u}_g u_l) + \bar{\chi}_x^a\alpha_g + \bar{\chi}_x^u(u_g - u_l) + \bar{\chi}_x^p p \\ \alpha_l\rho_l u_l^2 + \bar{\alpha}_l p - \bar{\chi}^{vm} k(\bar{u}_l u_g - \bar{u}_g u_l) - \bar{\chi}_x^a\alpha_g - \bar{\chi}_x^u(u_g - u_l) - \bar{\chi}_x^p p \end{bmatrix} \tag{D.10}$$

where

$$\bar{\chi}_x^a = \bar{\alpha}_g\bar{\alpha}_l(\bar{\rho}_g+\bar{\rho}_l)(\bar{u}_g-\bar{u}_l)^2 \tag{D.11}$$

$$\bar{\chi}_x^u = \bar{\alpha}_g\bar{\alpha}_l(\bar{\alpha}_g\bar{\rho}_l-\bar{\alpha}_l\bar{\rho}_g)(\bar{u}_g-\bar{u}_l) \tag{D.12}$$

$$\bar{\chi}_x^p = \bar{\alpha}_g\bar{\alpha}_l(\bar{\rho}_g+\bar{\rho}_l)(\bar{u}_g-\bar{u}_l)\left(\frac{\bar{\alpha}_g\bar{u}_g}{\bar{\rho}_g}\frac{1}{\bar{c}_g^2}+\frac{\bar{\alpha}_l\bar{u}_l}{\bar{\rho}_l}\frac{1}{\bar{c}_l^2}\right) \tag{D.13}$$

Considering the primitive variable $\mathbf{V}=[p,u_g,u_l,\alpha_g]^T$, the equation becomes:

$$\frac{\partial\mathbf{V}}{\partial t}+\frac{d\mathbf{V}}{d\mathbf{U}}\frac{d\mathsf{F}}{d\mathbf{V}}\frac{\partial\mathbf{V}}{\partial x}=\frac{d\mathbb{V}}{d\mathbf{U}}\mathbf{S} \tag{D.14}$$

and the matrix $d\mathbf{U}/d\mathbf{V}$ becomes:

$$\frac{d\mathbf{U}}{d\mathbf{V}}=\begin{bmatrix} \dfrac{\alpha_g}{c_g^2} & 0 & 0 & \rho_g \\ \dfrac{\alpha_l}{c_l^2} & 0 & 0 & -\rho_l \\ \dfrac{\alpha_g u_g}{c_g^2}+\chi_t^p & \alpha_g\rho_g+\chi^{vm}k & -\chi^{vm}k & \rho_g u_g \\ \dfrac{\alpha_l u_l}{c_l^2}-\chi_t^p & -\chi^{vm}k & \alpha_l\rho_l+\chi^{vm}k & -\rho_l u_l \end{bmatrix} \tag{D.15}$$

and $d\mathbf{V}/d\mathbf{U}$, the inverse of the above matrix, can be written:

$$\frac{d\mathbf{V}}{d\mathbf{U}}=\begin{bmatrix} \rho_l\dfrac{c_0^2}{\rho_s} & \rho_g\dfrac{c_0^2}{\rho_s} & 0 & 0 \\ \Psi_1 & \Psi_2 & \dfrac{\rho_l+\alpha_g k\rho}{\alpha_g\tilde{\rho}^2} & \dfrac{k\rho}{\tilde{\rho}^2} \\ \Psi_3 & \Psi_4 & \dfrac{k\rho}{\tilde{\rho}^2} & \dfrac{\rho_g+\alpha_l k\rho}{\alpha_l\tilde{\rho}^2} \\ \dfrac{\alpha_l c_0^2}{c_l^2\rho_s} & -\dfrac{\alpha_g c_0^2}{c_g^2\rho_s} & 0 & 0 \end{bmatrix} \tag{D.16}$$

where

$$\Psi_1 = -\frac{\alpha_l\rho_l(\rho_g+\rho_l)\Delta u}{\rho_g\tilde{\rho}^2}-\frac{u_g(\rho_l+\alpha_g k\rho)}{\alpha_g\tilde{\rho}^2}$$

$$\Psi_2 = -\frac{\alpha_l(\rho_g+\rho_l)\Delta u}{\tilde{\rho}^2}-\frac{k\rho u_l}{\tilde{\rho}^2}$$

$$\Psi_3 = \frac{\alpha_g(\rho_g+\rho_l)\Delta u}{\tilde{\rho}^2}-\frac{k\rho u_g}{\tilde{\rho}^2}$$

$$\Psi_4 = \frac{\alpha_g\rho_g(\rho_g+\rho_l)\Delta u}{\rho_l\tilde{\rho}^2}-\frac{u_l(\rho_g+\alpha_l k\rho)}{\alpha_g\tilde{\rho}^2}$$

and

$$\rho = \alpha_g \rho_g + \alpha_l \rho_l \tag{D.17}$$

$$\tilde{\rho}^2 = \rho_g \rho_l + k(\alpha_g \rho_g + \alpha_l \rho_l)^2 \tag{D.18}$$

The vector of flux F is given in (D.10) and the Jacobian matrix $d\mathsf{F}/d\mathbf{V}$ is:

$$\frac{d\mathsf{F}}{d\mathbf{V}} = \begin{bmatrix} \frac{\alpha_g u_g}{c_g^2} & \alpha_g \rho_g & 0 & \rho_g u_g \\ \frac{\alpha_l u_l}{c_l^2} & 0 & \alpha_l \rho_l & -\rho_l u_l \\ \alpha_g + \alpha_g \frac{u_g^2}{c_g^2} + \chi_x^p & 2\alpha_g \rho_g u_g + \chi_x^u + \chi^{vm} k u_l & -\chi_x^u - \chi^{vm} k u_g & \rho_g u_g^2 + \chi_x^a \\ \alpha_l + \alpha_l \frac{u_l^2}{c_l^2} - \chi_x^p & -\chi_x^u - \chi^{vm} k u_l & 2\alpha_l \rho_l u_l + \chi_x^u + \chi^{vm} k u_g & -\rho_l u_l^2 - \chi_x^a \end{bmatrix} \tag{D.19}$$

From the literature, $\mathbf{A}_p \equiv d\mathbf{V}/d\mathbf{U} \cdot d\mathsf{F}/d\mathbf{V}$ (Städtke, 2006), and substituting:

$$\mathbf{A}_p = \begin{bmatrix} u_g - \Delta u \frac{\alpha_l \rho_g c_0^2}{\rho_s c_l^2} & \alpha_g \rho_g \rho_l \frac{c_0^2}{\rho_s} & \alpha_l \rho_g \rho_l \frac{c_0^2}{\rho_s} & \rho_g \rho_l \Delta u \frac{c_0^2}{\rho_s} \\ \frac{\rho_l + k\rho}{\tilde{\rho}^2} & u_1 \frac{\rho_g \rho_l}{\tilde{\rho}^2} + u_2 \frac{k\rho^2}{\tilde{\rho}^2} & -\Delta u \frac{\alpha_l \rho_l (\rho_l + k\rho)}{\tilde{\rho}^2} & 0 \\ \frac{\rho_g + k\rho}{\tilde{\rho}^2} & \Delta u \frac{\alpha_g \rho_g (\rho_g + k\rho)}{\tilde{\rho}^2} & u_1 \frac{\rho_g \rho_l}{\tilde{\rho}^2} + u_2 \frac{k\rho^2}{\tilde{\rho}^2} & 0 \\ \frac{\alpha_g \alpha_l \Delta u}{c_g^2 c_l^2} \frac{c_0^2}{\rho_s} & \frac{\alpha_g \alpha_l \rho_g}{c_l^2} \frac{c_0^2}{\rho_s} & -\frac{\alpha_g \alpha_l \rho_l}{c_g^2} \frac{c_0^2}{\rho_s} & u_l + \Delta u \frac{\alpha_l \rho_g c_0^2}{\rho_s c_l^2} \end{bmatrix} \tag{D.20}$$

$$u_1 = \alpha_g u_g + \alpha_l u_l \qquad u_2 = \frac{\alpha_g \rho_g u_g + \alpha_l \rho_l u_l}{\alpha_g \rho_g + \alpha_l \rho_l}$$

The eigenvalues of the matrix A_p are:

$$\lambda_1 = u_g;\ \lambda_2 = u_l;\ \lambda_3 = u_s + c;\ \lambda_4 = u_s - c \tag{D.21}$$

The matrix of the corresponding right eigenvectors $\mathbf{R}_p$ can be solved (Städtke, 2006):

$$\mathbf{R}_p = \begin{bmatrix} \alpha_l\rho_l\Delta u^2 & \alpha_g\rho_g\Delta u^2 & \tilde{\rho}^2\mathcal{C}_0^2 & \tilde{\rho}^2\mathcal{C}_0^2 \\ 0 & -\Delta u & \tilde{\rho}_l(c-\tilde{\alpha}_l\Delta u) & \tilde{\rho}_l(-c-\tilde{\alpha}_l\Delta u) \\ \Delta u & 0 & \tilde{\rho}_g(c+\tilde{\alpha}_g\Delta u) & \tilde{\rho}_g(-c+\tilde{\alpha}_g\Delta u) \\ \alpha_l^2\dfrac{\Delta u^2}{c_l^2} - \alpha_l & \alpha_g - \alpha_g^2\dfrac{\Delta u^2}{c_g^2} & -\dfrac{\alpha_g\alpha_l c_0^2}{\rho_s}\left(\dfrac{\tilde{\rho}_g\rho_l}{c_g^2} - \dfrac{\rho_g\tilde{\rho}_l}{c_l^2}\right) & -\dfrac{\alpha_g\alpha_l c_0^2}{\rho_s}\left(\dfrac{\tilde{\rho}_g\rho_l}{c_g^2} - \dfrac{\rho_g\tilde{\rho}_l}{c_l^2}\right) \end{bmatrix} \tag{D.22}$$

with

$$\tilde{\rho}_g = \rho_g + k\rho \qquad \tilde{\rho}_l = \rho_l + k\rho$$

Rewriting the matrix $\mathbf{A}_p$:

$$\mathbf{A}_p = \mathbf{R}_p\Lambda\mathbf{R}_p^{-1} \tag{D.23}$$

where $\mathbf{\Lambda}$ is the diagonal matrix of eigenvalues.

Before introducing $\mathbf{R}_p^{-1}$, the matrix of the left eigenvector $\mathbf{R}_p^L$ can be obtained as in the literature (Städtke, 2006) by solving $\mathbf{R}_p^L\mathbf{A}_p = \mathbf{\Lambda}\mathbf{R}_p^L$:

$$\mathbf{R}_p^L = \begin{bmatrix} \alpha_g\dfrac{\Delta u}{c_g^2} & \alpha_g\rho_g & -\alpha_g\tilde{\rho}_l\dfrac{\rho_g}{\tilde{\rho}_g} & \rho_g\Delta u \\ \alpha_l\dfrac{\Delta u}{c_l^2} & \alpha_l\tilde{\rho}_g\dfrac{\rho_l}{\tilde{\rho}_l} & -\alpha_l\rho_l & -\rho_l\Delta u \\ c\tilde{\rho}_s + \Delta u\Delta\rho & \alpha_g\tilde{\rho}^2\left(c_2^2 + c\Delta u\dfrac{\rho_g\tilde{\rho}_s}{\tilde{\rho}^2}\right) & \alpha_l\tilde{\rho}^2\left(c_1^2 - c\Delta u\dfrac{\rho_l\tilde{\rho}_s}{\tilde{\rho}^2}\right) & \tilde{\rho}^2\Delta u\mathcal{C}_0^2 \\ -c\tilde{\rho}_s + \Delta u\Delta\rho & \alpha_g\tilde{\rho}^2\left(c_2^2 - c\Delta u\dfrac{\rho_g\tilde{\rho}_s}{\tilde{\rho}^2}\right) & \alpha_l\tilde{\rho}^2\left(c_1^2 + c\Delta u\dfrac{\rho_l\tilde{\rho}_s}{\tilde{\rho}^2}\right) & \tilde{\rho}^2\Delta u\mathcal{C}_0^2 \end{bmatrix} \tag{D.24}$$

where

$$\begin{aligned} c_1^2 &= c^2 - \frac{\alpha_g^2 \rho_g \rho_l \tilde{\rho}_l^2}{\tilde{\rho}^4} \Delta u^2 \\ c_2^2 &= c^2 - \frac{\alpha_l^2 \rho_g \rho_l \tilde{\rho}_g^2}{\tilde{\rho}^4} \Delta u^2 \\ \Delta\rho &= \alpha_g^2 \frac{\tilde{\rho}_l \mathcal{C}_0^2}{c_g^2} - \alpha_l^2 \frac{\tilde{\rho}_g \mathcal{C}_0^2}{c_l^2} \end{aligned}$$

and:

$$\tilde{\rho}_s = \rho_s + k\rho$$

A diagonal matrix $\mathbf{\Omega}$ is yielded by solving the product of $\mathbf{R}_p^L \cdot \mathbf{R}_p$, resulting in:

$$\begin{aligned} \omega_1 &= \alpha_l \Delta u^3 \frac{\rho_s}{c_0^2} - \Delta u \frac{\rho_g}{\tilde{\rho}_g} \tilde{\rho}_s; \\ \omega_2 &= \alpha_g \Delta u^3 \frac{\rho_s}{c_0^2} - \Delta u \frac{\rho_l}{\tilde{\rho}_l} \tilde{\rho}_s; \\ \omega_3 &= 2\tilde{\rho}^2 \tilde{\rho}_s c (c + \tilde{\alpha_g} \Delta u)(c - \tilde{\alpha_l} \Delta u); \\ \omega_4 &= 2\tilde{\rho}^2 \tilde{\rho}_s c (-c + \tilde{\alpha_g} \Delta u)(c + \tilde{\alpha_l} \Delta u) \end{aligned} \tag{D.25}$$

Rewriting the matrix $\mathbf{R}_p^L = [\mathcal{R}_1, \mathcal{R}_2, \mathcal{R}_3, \mathcal{R}_4]^T$ ($\mathcal{R}_i$ represents the ith row, where $i = 1$, 2, 3, or 4.), and $\mathbf{R}_p^{-1}$ can be obtained:

$$\mathbf{R}_p^{-1} = \begin{bmatrix} \mathcal{R}_1/\omega_1 \\ \mathcal{R}_2/\omega_2 \\ \mathcal{R}_3/\omega_3 \\ \mathcal{R}_4/\omega_4 \end{bmatrix} \tag{D.26}$$

if $\omega_i \neq 0$.

The Euler-like governing equations for the compressible two-fluid model can be written as:

$$\frac{\partial \mathbf{Q}}{\partial t} + \mathbf{C}_p \frac{\partial \mathbf{Q}}{\partial x} = \mathbf{S}_Q \tag{D.27}$$

The coefficients matrix, $\mathbf{C}_p = \mathbf{A} + \mathbf{B}$, can be written as:

$$\mathbf{C}_p = \frac{dQ}{dV} A_p \frac{dV}{dQ} \tag{D.28}$$

In the above equation, the matrix dQ/dV can be directly solved:

$$\frac{d\mathbf{Q}}{d\mathbf{V}} = \begin{bmatrix} \frac{\alpha_g}{c_g^2} & 0 & 0 & \rho_g \\ \frac{\alpha_l}{c_l^2} & 0 & 0 & -\rho_l \\ \frac{\alpha_g u_g}{c_g^2} & \alpha_g\rho_g & 0 & \rho_g u_g \\ \frac{\alpha_l u_l}{c_l^2} & 0 & \alpha_l\rho_l & -\rho_l u_l \end{bmatrix} \tag{D.29}$$

and its inverse is:

$$\frac{d\mathbf{V}}{d\mathbf{Q}} = \begin{bmatrix} \rho_l\frac{c_0^2}{\rho_s} & \rho_g\frac{c_0^2}{\rho_s} & 0 & 0 \\ -\frac{u_g}{\alpha_g\rho_g} & 0 & \frac{1}{\alpha_g\rho_g} & 0 \\ 0 & -\frac{u_l}{\alpha_l\rho_l} & 0 & \frac{1}{\alpha_l\rho_l} \\ \frac{\alpha_l c_0^2}{c_l^2\rho_s} & -\frac{\alpha_g c_0^2}{c_g^2\rho_s} & 0 & 0 \end{bmatrix} \tag{D.30}$$

The expanded form of the matrix $\mathbf{C}_p$ is:

$$\mathbf{C}_p = \begin{bmatrix} 0 & 0 & 1 & 0 \\ 0 & 0 & 0 & 1 \\ \tilde{\alpha}_g\rho_l\frac{c_0^2}{\rho_s} + \tilde{\alpha}_l u_g\Delta u - u_g^2 & \tilde{\alpha}_g\rho_g\frac{c_0^2}{\rho_s} + \tilde{\alpha}_g u_l\Delta u & 2u_g - \tilde{\alpha}_l\Delta u & -\tilde{\alpha}_g\Delta u \\ \tilde{\alpha}_l\rho_l\frac{c_0^2}{\rho_s} - \tilde{\alpha}_l u_g\Delta u & \tilde{\alpha}_l\rho_g\frac{c_0^2}{\rho_s} - \tilde{\alpha}_g u_l\Delta u - u_l^2 & \tilde{\alpha}_l\Delta u & 2u_l + \tilde{\alpha}_g\Delta u \end{bmatrix} \tag{D.31}$$

By recalling equation (D.23), the matrix $\mathbf{C}_p$ can be rewritten as:

$$\mathbf{C}_p = \mathbf{R}\cdot\mathbf{\Lambda}\cdot\mathbf{R}^{-1} = \frac{d\mathbf{Q}}{d\mathbf{V}}\mathbf{R}_p\cdot\mathbf{\Lambda}\cdot\mathbf{R}_p^{-1}\frac{d\mathbf{V}}{d\mathbf{Q}} \tag{D.32}$$

Similarly, the matrix of right eigenvectors, $\mathbf{R} = d\mathbf{Q}/d\mathbf{V}\cdot\mathbf{R}_p = [\mathbf{R}_1, \mathbf{R}_2, \mathbf{R}_3, \mathbf{R}_4]$, and $\mathbf{R}_i$ is the ith column (where $i = 1$, 2, 3, and 4):

$$\mathbf{R}_1 = \begin{bmatrix} \alpha_l\Delta u^2\dfrac{\rho_s}{c_0^2} - \alpha_l\rho_g \\ \alpha_l\rho_l \\ \alpha_l u_g\Delta u^2\dfrac{\rho_s}{c_0^2} - \alpha_l\rho_g u_g \\ \alpha_l\rho_l u_g \end{bmatrix} \qquad \mathbf{R}_2 = \begin{bmatrix} \alpha_g\rho_g \\ \alpha_g\Delta u^2\dfrac{\rho_s}{c_0^2} - \alpha_g\rho_l \\ \alpha_g\rho_g u_l \\ \alpha_g u_l\Delta u^2\dfrac{\rho_s}{c_0^2} - \alpha_g\rho_l u_l \end{bmatrix}$$

$$\mathbf{R}_3 = \begin{bmatrix} \alpha_g\rho_g\tilde{\rho}_l \\ \alpha_g\tilde{\rho}_g\rho_l \\ \alpha_g\rho_g\tilde{\rho}_l(c + u_g - \tilde{\alpha}_l\Delta u) \\ \alpha_g\tilde{\rho}_g\rho_l(c + u_l + \tilde{\alpha}_g\Delta u) \end{bmatrix} \mathbf{R}_4 = \begin{bmatrix} \alpha_g\rho_g\tilde{\rho}_l \\ \alpha_g\tilde{\rho}_g\rho_l \\ \alpha_g\rho_g\tilde{\rho}_l(-c + u_g - \tilde{\alpha}_l\Delta u) \\ \alpha_g\tilde{\rho}_g\rho_l(-c + u_l + \tilde{\alpha}_g\Delta u) \end{bmatrix} \tag{D.33}$$

And its inverse $\mathbf{R}^{-1} = \mathbf{R}_p^{-1}\cdot d\mathbf{V}/d\mathbf{Q} = [\mathbf{R}_1^I/\omega_1, \mathbf{R}_2^I/\omega_2, \mathbf{R}_3^I/\omega_3, \mathbf{R}_4^I/\omega_4]^T$ and $\mathbf{R}_i^I$ is the ith row (where $i = 1$, 2, 3, and 4.):

$$\begin{aligned}
\mathbf{R}_1^I &= \left[-u_l, \frac{\alpha_g\rho_g\tilde{\rho}_l}{\alpha_l\tilde{\rho}_g\rho_l}u_l, 1, -\frac{\alpha_g\rho_g\tilde{\rho}_l}{\alpha_l\tilde{\rho}_g\rho_l}\right]; \\
\mathbf{R}_2^I &= \left[-\frac{\alpha_l\tilde{\rho}_g\rho_l}{\alpha_g\rho_g\tilde{\rho}_l}u_g, u_g, \frac{\alpha_l\tilde{\rho}_g\rho_l}{\alpha_g\rho_g\tilde{\rho}_l}, -1\right]; \\
\mathbf{R}_3^I &= \Bigg[\mathcal{C}_0^2\frac{\tilde{\rho}^2}{\rho_g}(c + \tilde{\alpha}_g\Delta u - u_g) + \tilde{\rho}_s u_g\Delta u(-c + \tilde{\alpha}_l\Delta u), \\
&\quad \mathcal{C}_0^2\frac{\tilde{\rho}^2}{\rho_l}(c - \tilde{\alpha}_l\Delta u - u_l) + \tilde{\rho}_s u_l\Delta u(c + \tilde{\alpha}_g\Delta u), \\
&\quad \frac{\tilde{\rho}^2}{\rho_g}\left(c_2^2 + c\Delta u\frac{\rho_g\tilde{\rho}_s}{\tilde{\rho}^2}\right), \frac{\tilde{\rho}^2}{\rho_l}\left(c_1^2 - c\Delta u\frac{\rho_l\tilde{\rho}_s}{\tilde{\rho}^2}\right)\Bigg]; \\
\mathbf{R}_4^I &= \Bigg[\mathcal{C}_0^2\frac{\tilde{\rho}^2}{\rho_g}(-c + \tilde{\alpha}_g\Delta u - u_g) + \tilde{\rho}_s u_g\Delta u(c + \tilde{\alpha}_l\Delta u), \\
&\quad \mathcal{C}_0^2\frac{\tilde{\rho}^2}{\rho_l}(-c - \tilde{\alpha}_l\Delta u - u_l) + \tilde{\rho}_s u_l\Delta u(-c + \tilde{\alpha}_g\Delta u), \\
&\quad \frac{\tilde{\rho}^2}{\rho_g}\left(c_2^2 - c\Delta u\frac{\rho_g\tilde{\rho}_s}{\tilde{\rho}^2}\right), \frac{\tilde{\rho}^2}{\rho_l}\left(c_1^2 + c\Delta u\frac{\rho_l\tilde{\rho}_s}{\tilde{\rho}^2}\right)\Bigg];
\end{aligned} \tag{D.34}$$

The matrix arising from the non-conservative terms can be obtained by $B =$

$C - A$ (A is given in (4.20)):

$$\mathbf{B} = \begin{bmatrix} 0 & 0 & 0 & 0 \\ 0 & 0 & 0 & 0 \\ \tilde{\alpha}_g\rho_l\dfrac{c_0^2}{\rho_s} + \tilde{\alpha}_l u_g \Delta u & \tilde{\alpha}_g\rho_g\dfrac{c_0^2}{\rho_s} + \tilde{\alpha}_g u_l \Delta u & -\tilde{\alpha}_l\Delta u & -\tilde{\alpha}_g\Delta u \\ \tilde{\alpha}_l\rho_l\dfrac{c_0^2}{\rho_s} - \tilde{\alpha}_l u_g \Delta u & \tilde{\alpha}_l\rho_g\dfrac{c_0^2}{\rho_s} - \tilde{\alpha}_g u_l \Delta u & \tilde{\alpha}_l\Delta u & \tilde{\alpha}_g\Delta u \end{bmatrix} \tag{D.35}$$

The matrix $d\mathbf{Q}/d\mathbf{U} = d\mathbf{Q}/d\mathbf{V} \cdot d\mathbf{V}/d\mathbf{U}$ is given as:

$$\frac{d\mathbf{Q}}{d\mathbf{U}} = \begin{bmatrix} 1 & 0 & 0 & 0 \\ 0 & 1 & 0 & 0 \\ \Phi_1 & \Phi_2 & \dfrac{\rho_g(\rho_l + \alpha_g k\rho)}{\tilde{\rho}^2} & \dfrac{\alpha_g\rho_g k\rho}{\tilde{\rho}^2} \\ -\Phi_1 & -\Phi_2 & \dfrac{\alpha_l\rho_l k\rho}{\tilde{\rho}^2} & \dfrac{\rho_l(\rho_g + \alpha_l k\rho)}{\tilde{\rho}^2} \end{bmatrix} \tag{D.36}$$

where

$$\begin{aligned} \Phi_1 &= \frac{\alpha_l\rho_l k\rho}{\tilde{\rho}^2}u_g - \frac{\alpha_g\alpha_l\rho_l(\rho_g + \rho_l)}{\tilde{\rho}^2}\Delta u \\ \Phi_2 &= -\frac{\alpha_g\rho_g k\rho}{\tilde{\rho}^2}u_l - \frac{\alpha_g\alpha_l\rho_g(\rho_g + \rho_l)}{\tilde{\rho}^2}\Delta u \end{aligned}$$

Paper I

Iterative versus Non-iterative Numerical Schemes for One-Dimensional Compressible Transient Flow Part I: Isothermal Flow

Xiaoju Du and Ole Jørgen Nydal

Submitted to International Journal of Multiphase Flow

Is not included due to copyright

Paper II

Iterative versus Non-iterative Numerical Schemes for One-Dimensional Compressible Transient Flow Part II: Thermal Flow

Xiaoju Du and Ole Jørgen Nydal

Submitted to International Journal of Multiphase Flow

Is not included due to copyright

Paper III

Staggered and Non-staggered Numerical Schemes for Two-Phase Transient Flow

Xiaoju Du and Ole Jørgen Nydal

Submitted to Journal of Scientific Computing

Is not included due to copyright